

Article

Mirror Symmetry Breaking in Helical Polysilanes: Preference between Left and Right of Chemical and Physical Origin

Michiya Fujiki

Graduate School of Materials Science, Nara Institute of Science and Technology (NAIST), 8916-5 Takayama, Ikoma, Nara 630-0036, Japan; E-Mail: fujikim@ms.naist.jp

Received: 21 February 2010; in revised form: 2 August 2010 / Accepted: 9 August 2010 /

Published: 13 August 2010

Abstract: From elemental particles to human beings, matter is dissymmetric with respect to mirror symmetry. In 1860, Pasteur conjectured that biomolecular handedness—homochirality—may originate from certain inherent dissymmetric forces existing in the universe. Kipping, a pioneer of organosilicon chemistry, was interested in the handedness of sodium chlorate during his early research life. Since Kipping first synthesized several Si-Si bonded oligomers bearing phenyl groups, Si-Si bonded high polymers carrying various organic groups—polysilanes—can be prepared by sodium-mediated condensation of the corresponding organodichlorosilanes. Among these polysilanes, optically active helical polysilanes with enantiomeric pairs of organic side groups may be used for testing the mirror symmetry-breaking hypothesis by weak neutral current (WNC) origin in the realm of chemistry and material science. Several theoretical studies have predicted that WNC-existing chiral molecules with stereogenic centers and/or stereogenic bonds allow for distinguishing between image and mirror image molecules. Based on several amplification mechanisms, theorists claimed that minute differences, though still very subtle, may be detectable by precise spectroscopic and physicochemical measurements if proper chiral molecular pairs were employed. The present paper reports comprehensively an inequality between six pairs of helical polysilane high polymers, presumably, detectable by (chir)optical and achiral $^{29}\text{Si}/^{13}\text{C}$ -NMR spectra, and viscometric measurements.

Keywords: parity violation; helix; polysilane; optically active; polymer; phase transition; circular dichroism; NMR; viscometry; Salam; weak neutral current

1. Introduction

Why does matter dominantly exist in the universe? Why is the universe inherently chiral and asymmetric? What is the origin of biomolecular handedness in life—homochirality—on the blue planet? Several explanations have already been proposed for these questions and can be seen in many monographs and reviews [1–48]. Except for achiral glycine, the amino acids in proteins are all in their L-form. Some of these ideas rely on a matter of chance to induce the preference—an event of spontaneous symmetry breaking. Others believe that the fundamental lack of mirror image symmetry in the early Earth inevitably led to the L-preference. Although it is now established that left–right symmetry is broken at the level of interactions between subatomic particles and atomic vapor. However, detection of dissymmetry at the molecular scale remains a challenging issue.

Homochirality, though *de facto*, is a long-standing puzzle raising curiosity among scientists since the 19th century [1,19,24]. In 1860, Pasteur alleged that homochirality originates from the demarcation line between the animate and inanimate worlds. He conjectured that biomolecular homochirality arises from an inherent universal dissymmetry force. He inferred the concept of broken mirror symmetry by physical origins, including circularly polarized light and a static magnetic field, although there was no theoretical or experimental evidence at that time. Most chemists and physicists believed that nature's laws cannot distinguish between left and right in all physical properties and chemical processes.

Kipping, a pioneer of organosilicon and polysilane chemistry, and Pope assumed that biomolecular homochirality is applicable to purely inorganic substances. They examined thousands of crystals produced from achiral NaClO_3 (molecular symmetry, C_{3v} , but, crystal exists as D- and L-forms) to test the preference between left and right by mirror symmetry-breaking crystallization [1]. However, they did not conclude that the broken mirror symmetry crystallization occurs by the expected inherent physical origins because the events appear to be a statistical distribution—a matter of chance.

Physicists invented three discrete symmetries (C ; charge, P ; parity, T ; time) and their combination symmetries (CP , PT , CT , and CPT) to understand nature's laws [24,48,49]. Physicists in the mid-20th century knew four fundamental forces (gravity, weak force, strong force, and electromagnetic force) governing matter and universe. Since the first paper describing P -symmetry conservation—the concept of the mirror symmetry—by Wigner in 1927 [49,50], they had long accepted this concept as being axiomatic in developing theories for explaining phenomena. However, violations of C , P , T , and CP symmetries at the levels of elemental particles and upward constitute the most fundamental concept in modern physics [51,52], since the broken P -symmetry at subatomic level was proven experimentally by Wu *et al.* in 1957 [53] to verify the P -symmetry conservation, which had been questioned by Lee and Yang in 1956 [54].

Nambu demonstrated the idea of "spontaneous symmetry breaking" in the 1960s [55,56]. His work led to the standard model in particle physics developed by Weinberg [57], Salam [58], and Glashow [59]. The standard model unifying the parity-violating (PV) weak force and parity-conserving (PC) electromagnetic force led to the idea of an electroweak (EW) force, which may not be familiar with chemists and material scientists. The existence of three massive W^\pm and Z^0 bosons along with a massless photon predicted by the model was proven by an international team at CERN in 1983 [60]. Scientists interested in the origin of biomolecular handedness assume that the PV -weak neutral current (WNC)

mediated by massive neutral Z^0 boson is intimately connected to the mirror symmetry breaking at the closed-shell biomolecular level as well as the atomic parity violation (APV) [61,62].

In chemistry, bioscience, and material science, left and right can interchange through a mirror. Many physical properties of materials and chemical reactions obey mirror symmetry-based physics laws. A pair of image and mirror image molecules—enantiomers—shows no differences in melting point, boiling point, and spectroscopic properties that involve electronic transition energies, vibrational frequencies, and magnetic resonance frequencies. The pair should exhibit exactly equal intensities with opposite signs in circular dichroism (CD) and optical rotation in electronic and vibrational regions due to the *PC* electromagnetic force in physical and chemical processes.

However, modern theoretical studies [11–18,19–23,26,28,30,31,33,36–41,43,44,46] have claimed that an image and its mirror molecule are no longer enantiomers due to an energy inequality induced by the existence of *PV-WNC*. Due to a parity-violating energy shift (*PVES*) of the electronic binding energy with a positive value, $+E_{PV}$, for the image molecule and a *PVES* with a negative value, $-E_{PV}$, for the mirror image molecule, or *vice versa*, *PVES* makes the pair become a diastereomer, exhibiting subtle differences in physical properties and chemical processes. The parity-violating energy difference (*PVED*) between image and mirror image molecules is given as $PVED = E_{PV} - (-E_{PV}) = 2 \cdot E_{PV}$. Numbers of theoretical studies have discussed that the occurrence of *PVES* may appear spectroscopically as slight differences in electronic transition energies [13,16,20], vibrational frequencies [43], ro-vibrational frequencies [17,41], NMR chemical shifts [21], circular polarization in electronic transition and vibrational frequency regions [18,43], a concept hereafter called the molecular parity violation (*MPV*) hypothesis in this article.

Because of the extremely small *PVED* of $\sim 10^{-19}$ eV and negligibly small 10^{-15} %*ee* [13], *PV-WNC* cannot induce any observable *MPV* effects. In the molecules containing heavy elements, *PVED* may increase up to $\sim 10^{-14}$ eV due to the heavy element effect [43], yet it still remains undetectable. Thus far, several amplification models, including polymerization and crystallization [5], molecules with heavier atoms [20], tunneling and oscillating between left and right in a double well [11], non-equilibrium autocatalytic chemical reactions [15,38], and second-order phase transition systems [26], have been proposed.

Several experimental results testing the *MPV* hypothesis have been reported so far. Based on the Salam's hypothesis describing that homochirality is the consequence of the cooperative second-order phase transition of an electron-neutron pair [26], Wang *et al.* examined a pair of D- and L-alanine single crystals by means of Raman, NMR, neutron scattering, supersonic wave, magnetic susceptibility, and calorimeter [63]. She claimed the detection of subtle differences in physical properties between the D- and L-crystals below 270 K. Although these results were verified by other independent research groups, Compton and Schwerdtfeger [64], and Wilson *et al.* [65] did not agree with her claim due to a lack of reproducibility. They ascribed her results to certain impurities incorporated in non-naturally occurring alanine, crystal imperfection, and restricted motions in the solid crystals. To achieve discrete molecular systems in dilute gas phase, enabling the avoidance of molecular collisions, a few research groups are continuing to detect minute differences between images and mirror images using ultrahigh-resolution laser spectroscopy in mid-IR and far-IR regions [43]. More recently, Schwerdtfeger *et al.* predicted theoretically the large *MPV* effects for the chiral NWHCI molecule from relativistic density functional theory, revealing mirror symmetry breaking in N–W stretching frequency of 0.7 Hz

in IR region. Because this value could be detectable by an ultrahigh-resolution CO₂ laser spectrometer [66], the work was highlighted as a cover picture of a chemistry journal.

In 2006, Shinitzky *et al.* reported the subtle differences in helix-coil transition behaviors of D- and L-oligopeptides in water, as characterized by CD and isothermal titration calorimetry experiments [67]. They ascribed the differences to *ortho* (triplet, ↑↑) and *para* (singlet, ↑↓) nuclear spin states of water protons and the methylene protons of amino acids. Lahav and Schurig failed to reproduce Shinitzky's results [68]. Schwerdtfeger *et al.* claimed that several MPV-related experimental results are weakly based theoretically [69]. On the other hand, in 2008, Pomonis *et al.* reported that the α-helical motif in poly-D-glutamic acid is stable thermally, compared to that of poly-L-glutamic acid. Pomonis *et al.* ascribed this difference to an increased interaction of the L-species with more abundant *ortho*-water, in support of the Shinitzky's claim [70].

Although conclusive results using common chemical substances and apparatuses have not yet been reported, these modern MPV theories and current experimental reports, though still controversial, stimulated the author to revisit the equality and inequality of several ambidextrous artificial helical Si–Si bonded polymer–polysilanes–in solution as a function of temperature [71,72]. In a previous communication, the author reported preliminary testing results, implicating a possibility of detecting subtle differences in chiroptical and achiral ²⁹Si-NMR and viscometric data for a pair of helical polysilanes [73]. The present paper reported comprehensively the experimental tests of an equality and an inequality observed in chiroptical, ²⁹Si-/¹³Si-NMR, and viscometric measurements for six pairs of helical polysilanes carrying ambidextrous chiral side groups.

2. Results and Discussion

A family of polysilanes (Figure 1), compound **1** which is symmetrically substituted with chiral side groups, and compounds **2–6** which are asymmetrically substituted with chiral and achiral side groups, has several advantages for testing the MPV hypothesis because:

(i) The ambidextrous (*S*)- and (*R*)-3,7-dimethyloctyl moieties derive from highly pure β-citronellol available commercially from Fluka and/or Sigma-Aldrich. The use of β-citronellols allows for the ability to test the present results in any laboratory. By contrast, (*R*)-2-methylbutanol is not available commercially, and was obtained from custom synthesis by Chemical Soft (Kyoto, Japan) while (*S*)-2-methylbutanol is commercially available (TCI).

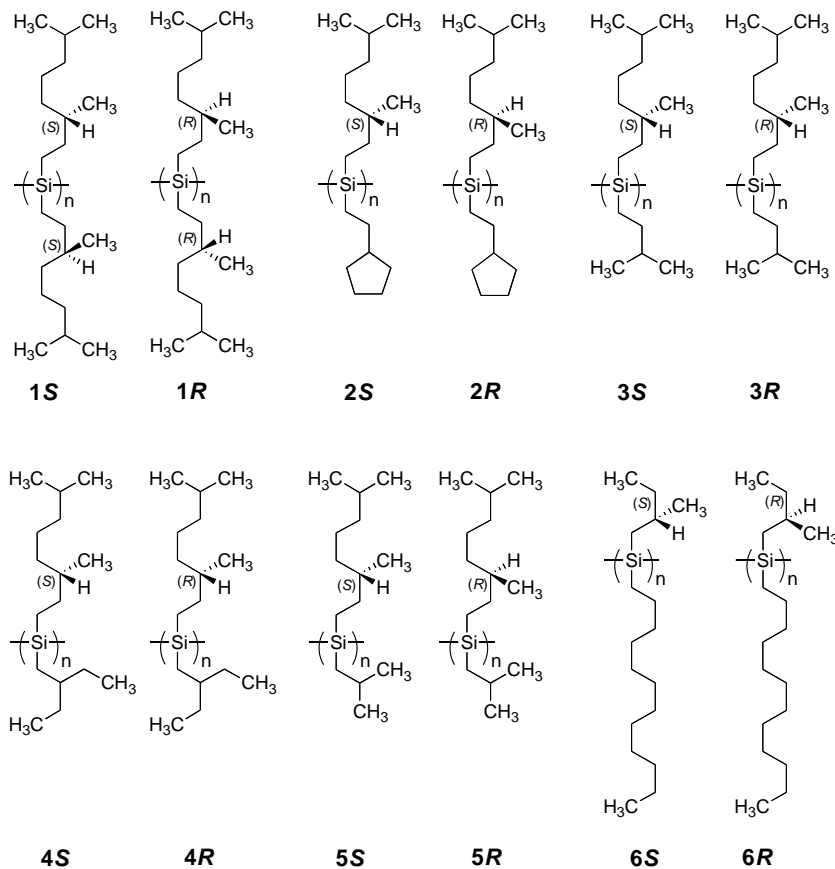
(ii) The Cotton CD signals of the helical polysilanes completely match the profiles of the corresponding Siσ–Siσ* absorptions (the electrically allowed S₀–S₁ transitions) in the near-UV region [71]. To evaluate the MPV effect induced by WNC (intrinsic chiral physical origins), excluding the effects caused by the PC electromagnetic force (conventional chiral chemical origins), we can compare the apparent dimensionless Kuhn's dissymmetry factors between a pair of helical polysilanes in isotropic solution, which are defined as $g_{CD} = \Delta\epsilon/\epsilon$, where $\Delta\epsilon$ and ϵ are the apparent CD and UV intensities [72,74]. The value of g_{CD} is independent of sufficiently high molecular weight (M_w), although both $\Delta\epsilon$ and ϵ depend somewhat on M_w [71]. The apparent g_{CD} values may be directly connected to the sum and/or subtraction of the $|g_{PV}|$ and $|g_{PC}|$ terms for the helical polysilane pairs. The values of g_{PV} and g_{PC} are dissymmetry factors of the PV and PC terms, respectively. The difference in population between the *P*- (dihedral angle (θ) ~150°) and *M*- (θ ~210°) motifs for the polysilane pairs is directly associated with

the g_{PV} and g_{PC} values. The g_{PV} term, induced by ΔE_{PV} with the same magnitude but opposite sign for the pairs, contributes to the apparent g_{CD} value.

(iii) Helical polysilanes in a double well with a small barrier height of 2–3 kcal per Si–Si unit [75] exhibit an energy splitting energy, allowing quantum tunneling between *P*- and *M*-helices [11]. The tunneling between *P* and *M* permits an effective mixing between weak and electromagnetic forces because outer- and inner-shell electrons have an opportunity to interact with nucleons. This is important for electrons and nucleons because weak forces mediated by massive Z_0 bosons are effective only to neighbors within ultrashort-range interactions of $\sim 10^{-18}$ m [13,23].

(iv) Heavier Si nuclei (natural abundance of ^{28}Si 92.2 % (spin: 0, NMR inactive), ^{29}Si 4.7% (spin: $-1/2$, NMR active), and ^{30}Si 3.1% (spin: 0, NMR inactive) containing 14 protons and 14–16 neutrons and effective repeating numbers (N_{eff}) of up to $\sim 10^4$ [5] may linearly enhance ΔE_{pv} in comparison to the C–C bonded organic small molecules. The value of ΔE_{pv} is proportional to $N_{\text{eff}} \cdot Z^5$, while Z^3 is due to the *WNC* interaction and Z^2 , the spin-orbit interaction (where Z is the atomic number) [13,43]. A preliminary expected advantage ratio, $g_{\text{adv}} = \Delta E_{pv}/kT \sim 10^{-12}$ at 300 K, may sufficiently exceed the detectable *PNC* limit with a critical g_{adv} of $\sim 10^{-17}$ [15,16,22]. By comparing ^{29}Si -NMR spectra, the degree of main chain mobility is detectable as the difference in linewidth; the sum of the shielding and deshielding terms by inner-shell electrons of the main chain could be measurable as changes in chemical shifts [21].

Figure 1. Chemical structures of the six helical polysilane pairs tested in this work.

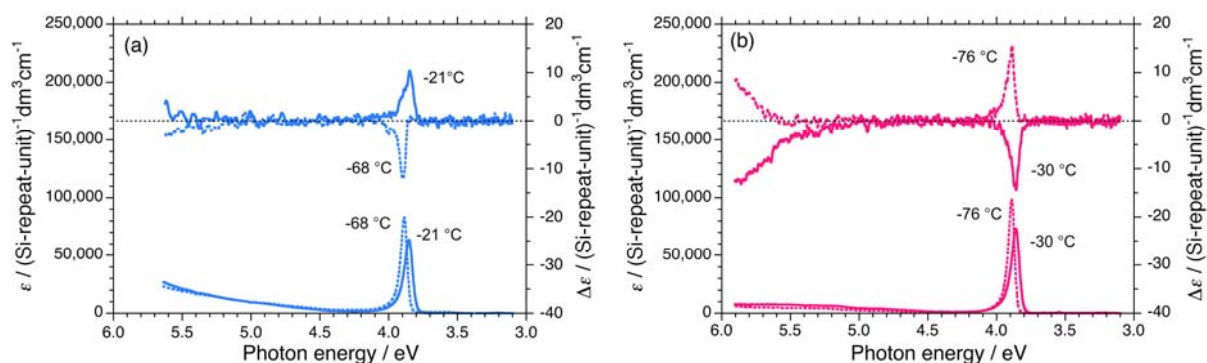


2.1. Chiroptical Spectral Analysis

2.1.1. Helical Polysilane Symmetrically Substituted with Chiral Side Groups in Isotropic Solution

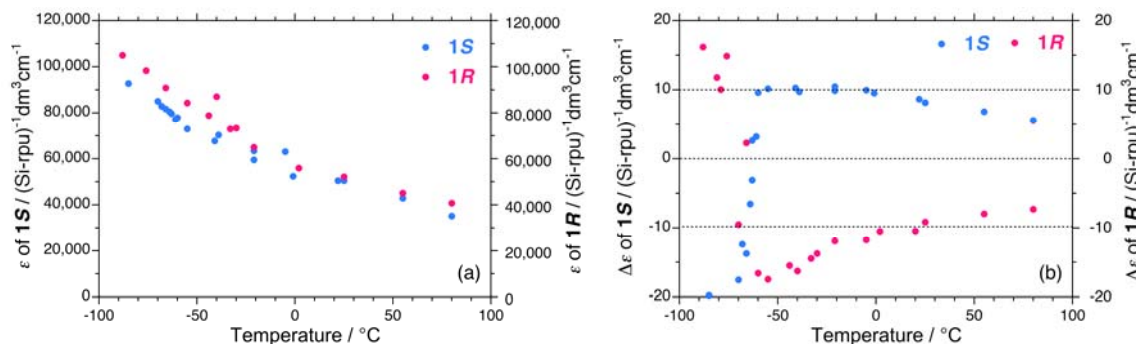
A comparison of UV and CD spectra between **1S** and **1R** in isooctane below and above the helix-helix transition temperature (T_c) of $-65\text{ }^\circ\text{C}$ is shown in Figure 2. The negatively signed Cotton CD signal of **1S** with an extremum of 3.90 eV at $-68\text{ }^\circ\text{C}$ is almost the inverse of the positively signed Cotton CD signal with an extremum of 3.85 eV at $-21\text{ }^\circ\text{C}$ over the whole 3.0 eV to 5.5 eV range. Conversely, the positively signed CD signal of **1R** with an extremum of 3.89 eV at $-76\text{ }^\circ\text{C}$ is almost the inverse of the negatively signed CD signal with an extremum of 3.87 eV at $-30\text{ }^\circ\text{C}$. Evidently, **1S** and **1R** undergo a helix-helix transition between the two temperatures.

Figure 2. UV and CD spectra in isooctane of (a) **1S** ($M_w = 863,000$, $M_n = 147,000$) at $-88\text{ }^\circ\text{C}$ and $-21\text{ }^\circ\text{C}$, and (b) **1R** ($M_w = 394,000$, $M_n = 85,800$) at $-76\text{ }^\circ\text{C}$ and $-10\text{ }^\circ\text{C}$.



The magnitudes of the UV and CD signal intensities near 3.9 eV of **1S** and **1R** in isooctane as a function of temperature are shown in Figure 3. The UV intensities of **1S** are somewhat weak compared to those of **1R** in the range of $-90\text{ }^\circ\text{C}$ to $+80\text{ }^\circ\text{C}$. However, the absolute magnitudes of the CD signals are intense in the negative CD region regardless of the side chirality and temperature.

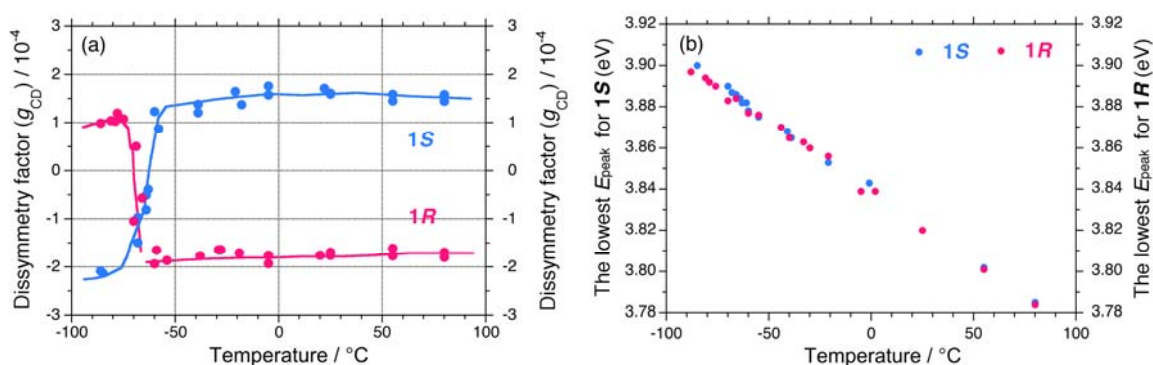
Figure 3. The magnitudes of the (a) UV absorptivity and (b) CD signal near 3.9 eV of **1S** ($M_w = 863,000$, $M_n = 147,000$) and **1R** ($M_w = 394,000$, $M_n = 85,800$) in isooctane as a function of temperature.



This tendency is evident when compared to the absolute magnitudes of the apparent g_{CD} values, $|g_{CD}|$. The values of g_{CD} near 3.9 eV for **1S** and **1R** in isooctane as a function of temperature are shown in Figure 4(a). Evidently, **1S** and **1R** undergo a cooperative, second-order helix-helix transition around -65 °C. In the range of -90 °C to -70 °C, the $|g_{CD}|$ values of **1S** are greater than those of **1R**, whereas in the range of -50 °C to $+80$ °C, the $|g_{CD}|$ values of **1S** are smaller than those of **1R**.

The differences in the $|g_{CD}|$ values are possible to relate with the observable contribution from the $2 \cdot |g_{PV}|$ term arising from the subtraction between the $(|g_{PC}| - |g_{PV}|)$ and $(|g_{PC}| + |g_{PV}|)$ terms of **1S** and **1R** in the range of -90 °C to -70 °C and between the $(|g_{PC}| + |g_{PV}|)$ and $(|g_{PC}| - |g_{PV}|)$ terms of **1S** and **1R** in the range of -50 °C to $+80$ °C. Regardless of the solution temperatures, the sign of $|g_{PV}|$ is negative, suggesting a preference for left-handed helicity (minus, *M*) rather than right-handed helicity (plus, *P*) in isooctane. The lowest exciton peak energies (E_{peak}) for **1S** and **1R** in isooctane as a function of temperature are not significantly different [Figure 4(b)].

Figure 4. (a) Apparent g_{CD} values near 3.9 eV and (b) apparent lowest exciton peak energies of **1S** ($M_w = 863,000$, $M_n = 147,000$) and **1R** ($M_w = 394,000$, $M_n = 85,800$) in isooctane as a function of temperature.

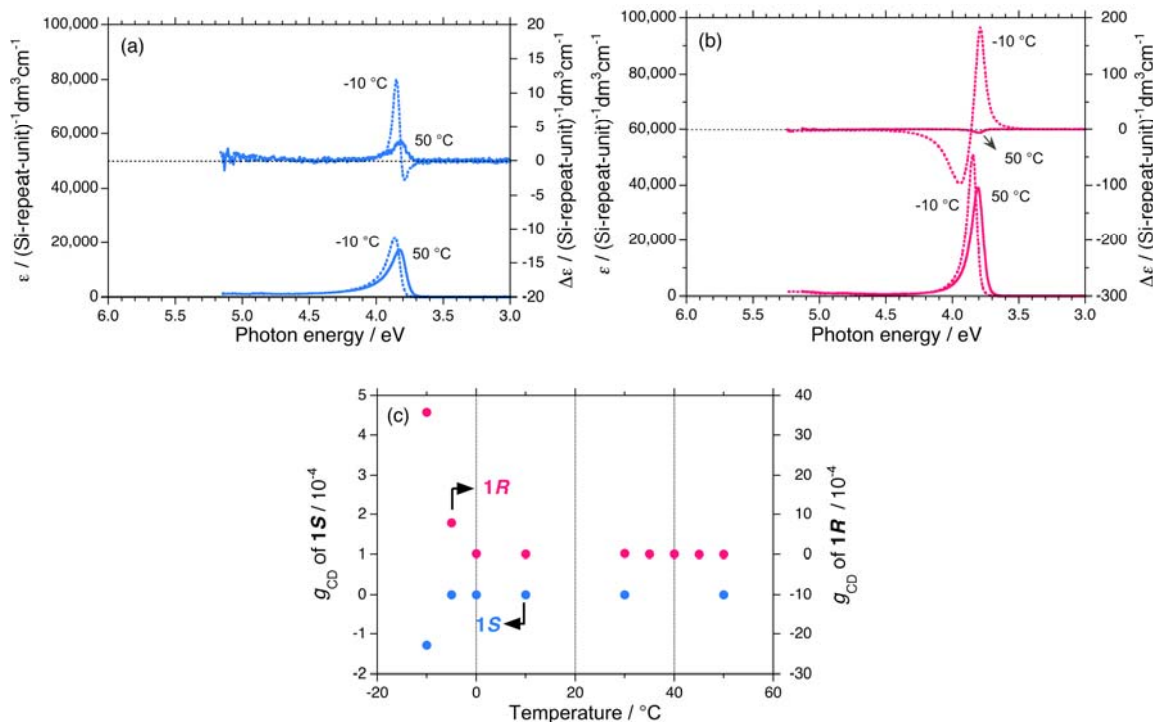


2.1.2. Helical Polysilane Aggregates Dispersed in Solution

The subtle differences in the $|g_{CD}|$ values between **1S** and **1R** dissolved in isotropic isooctane are recognized. However, the significant difference in the $|g_{CD}|$ values between **1S** and **1R** when dispersed as aggregate particles in isotropic chloroform is more evident. The aggregates spontaneously form when the polymer sample solution temperature is decreased. The bisignate CD signal originates from the so-called exciton-coupling signal of the Si–Si main chain chromophore in the aggregates.

A bisignate CD signal of **1S** aggregates with extrema of 3.80 eV (negative) and 3.85 eV (positive) appears at -10 °C while **1S** dissolved in chloroform at 50 °C exhibits a single CD signal with an extremum of 3.82 eV (positive) [Figure 5(a)]. Similarly, the bisignate CD signal of **1R** aggregates with extrema of 3.79 eV (positive) and 3.85 eV (negative) appears at -10 °C, while **1R** dissolved in chloroform at 50 °C exhibits a single CD signal with an extremum of 3.81 eV (negative) [Figure 5(b)]. The $|g_{CD}|$ value at the first Cotton CD band near 3.8 eV of **1S** and **1R** in chloroform in the range of -10 °C to $+50$ °C is plotted in Figure 5(c). The $|g_{CD}|$ value of **1R** at -10 °C is approximately 30-times more intense than that of **1S** at -10 °C. The difference in the $|g_{CD}|$ values of **1S** and **1R** was significantly more amplified for the aggregate forms than those molecularly dissolved in solution.

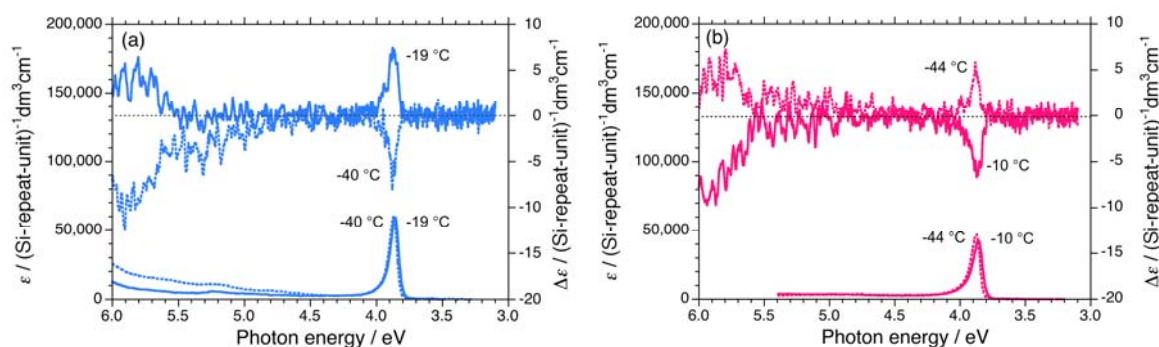
Figure 5. UV and CD spectra in chloroform of (a) **1S** ($M_w = 140,000$, $M_n = 34,400$) at -10 °C and $+50$ °C, and (b) **1R** ($M_w = 149,000$, $M_n = 39,500$) at -10 °C and $+50$ °C. (c) Apparent g_{CD} values near 3.8 eV of **1S** and **1R** aggregates dispersed in chloroform as a function of temperature.



2.1.3. Helical Polysilanes Asymmetrically Substituted with Chiral and Achiral Side Groups in Isotropic Solution

Three polysilanes (**2S/2R**, **3S/3R**, **4S/4R**) asymmetrically substituted with the chiral (*S*)-/*(R)*-3,7-dimethyloctyl and the achiral cyclopentaneethyl, 3-methylpentyl, and 2-ethylbutyl side groups undergo helix-helix transitions in isoctane [73]. The T_c s of **2**, **3**, and **4** increase in the order of -33 °C, -22 °C, and -7 °C, respectively. The UV and CD spectra of **2S/2R**, **3S/3R**, and **4S/4R** in isoctane below and above T_c are displayed in Figures 6(a)–6(b) and Appendix Figures A1(a)–1(d).

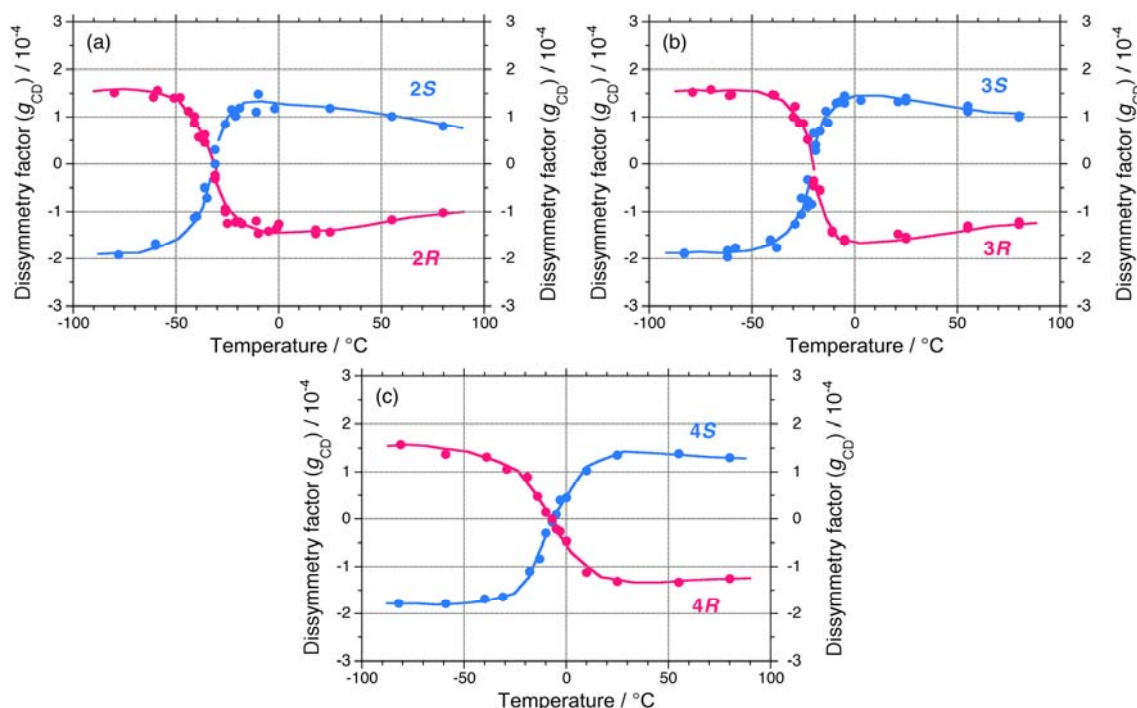
Figure 6. UV and CD spectra in isoctane of (a) **2S** ($M_w = 93,100$, $M_n = 57,900$) at -40 °C and -19 °C and (b) **2R** ($M_w = 51,800$, $M_n = 25,200$) at -44 °C and -10 °C.



The apparent g_{CD} values near 3.9 eV of **2S/2R**, **3S/3R**, and **4S/4R** in isoctane as a function of temperature are shown in Figures 7(a)–7(c), respectively. The $|g_{CD}|$ values of **2**, **3**, and **4** are considerably more intense in the negative CD region, regardless of the side chain chirality and temperature. Above the T_{cS} , the $|g_{CD}|$ values of **2**, **3**, and **4** carrying the (*R*)-group are greater than those with the (*S*)-group. By contrast, below the T_{cS} , the $|g_{CD}|$ values of **2**, **3**, and 4 carrying the (*S*)-group are greater than those with the (*R*)-group. These features of **2**, **3**, and **4** are identical to those of **1**.

On the other hand, **5** and **6** do not undergo helix-helix transitions in the range of -80 °C and $+80$ °C. However, even the **5S/5R** pair gives weak, but detectable differences in their chiroptical properties at low temperatures. The UV and CD spectra of the **5S/5R** pair in isoctane at low and high temperatures are displayed in Appendix Figures A1(e)–A1(f). The $|g_{CD}|$ value of **5R** at -80 °C is more intense than that of **5S** at -80 °C (Figure 7(a)), whereas the $|g_{CD}|$ values of **1–4** with the (*S*)-group at -80 °C are more intense than those of **1–4** with the (*R*)-group at -80 °C. Therefore, regardless of the side chain chirality, the $|g_{CD}|$ values of **1–5** at -80 °C are intensely negative, preferring *M*-screw-sense (Table 1).

Figure 7. Apparent g_{CD} values near 3.9 eV in isoctane as a function of temperature of (a) **2S** ($M_w = 93,100$, $M_n = 57,900$) and **2R** ($M_w = 51,800$, $M_n = 25,200$), (b) **3S** ($M_w = 232,000$, $M_n = 78,900$) and **3R** ($M_w = 156,000$, $M_n = 76,800$), and (c) **4S** ($M_w = 14,500$, $M_n = 11,300$) and **4R** ($M_w = 19,000$, $M_n = 15,200$).



A non-helix-helix-transitioned pair (**6S/6R**) exhibited subtle differences in chiroptical properties. The UV and CD spectra of the **6S/6R** pairs in isoctane at lower and higher temperatures are displayed in Appendix Figures A1(g)–A1(h). Although the $|g_{CD}|$ value of the negative CD band of **6R** are almost identical to those of **6S** in the range of -5 °C to $+80$ °C [Figure 8(b)], and the magnitudes of the UV and CD intensities of **6S** are slightly greater than those of **6R** in the range of -5 °C to $+80$ °C [Appendix Figure A2(a)]. The lowest Cotton CD extremum energies of **6S** and **6R** depend on the solution temperature in the range of -5 °C to $+80$ °C [Appendix Figure A2(b)].

Figure 8. Apparent g_{CD} values near 3.9 eV in isoctane as a function of temperature of (a) **5S** ($M_w = 42,300$, $M_n = 23,500$) and **5R** ($M_w = 36,900$, $M_n = 19,000$) and (b) **6S** ($M_w = 108,000$, $M_n = 37,300$) and **6R** ($M_w = 80,900$, $M_n = 34,600$).

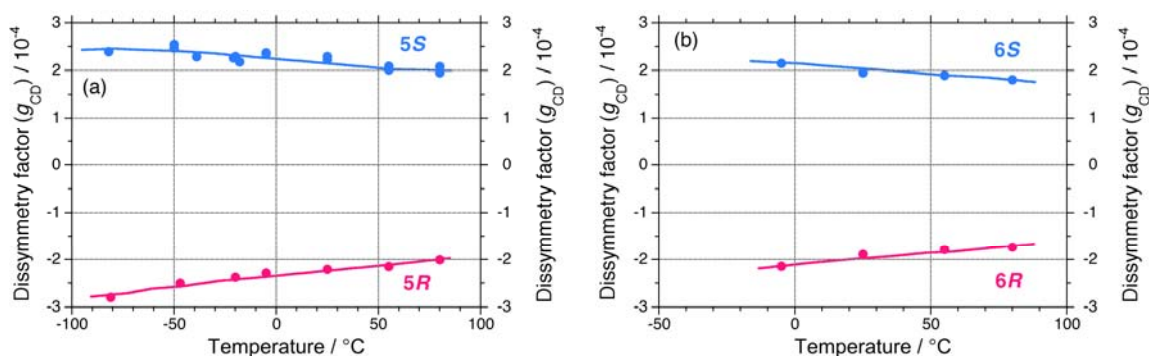


Table 1. Chiroptical parameters (g_{CD} , $|g_{PC}|$, g_{PV} values in 10^{-4}) of six polysilanes in isoctane.

Sample	$T_c / ^\circ\text{C}$	g_{CD} at -80°C	g_{CD} at $+80^\circ\text{C}$	$ g_{PC} / g_{PV}$ at -80°C	$ g_{PC} / g_{PV}$ at $+80^\circ\text{C}$
1S	-65	-2.11	+1.52	1.82 / -0.30	1.63 / -0.11
1R	-65	+1.52	-1.74		
2S	-33	-1.95	+0.81	1.74 / -0.21	0.94 / -0.13
2R	-33	+1.53	-1.07		
3S	-22	-1.90	+1.04	1.72 / -0.18	1.13 / -0.08
3R	-22	+1.53	-1.21		
4S	-7	-1.78	+1.33	1.68 / -0.10	1.30 / +0.03
4R	-7	+1.58	-1.26		
5S	-	+2.36	+1.95	2.57 / -0.21	1.98 / -0.02
5R	-	-2.78	-2.00		
6S	-	-	+1.79	-	-
6R	-	-	-1.71		

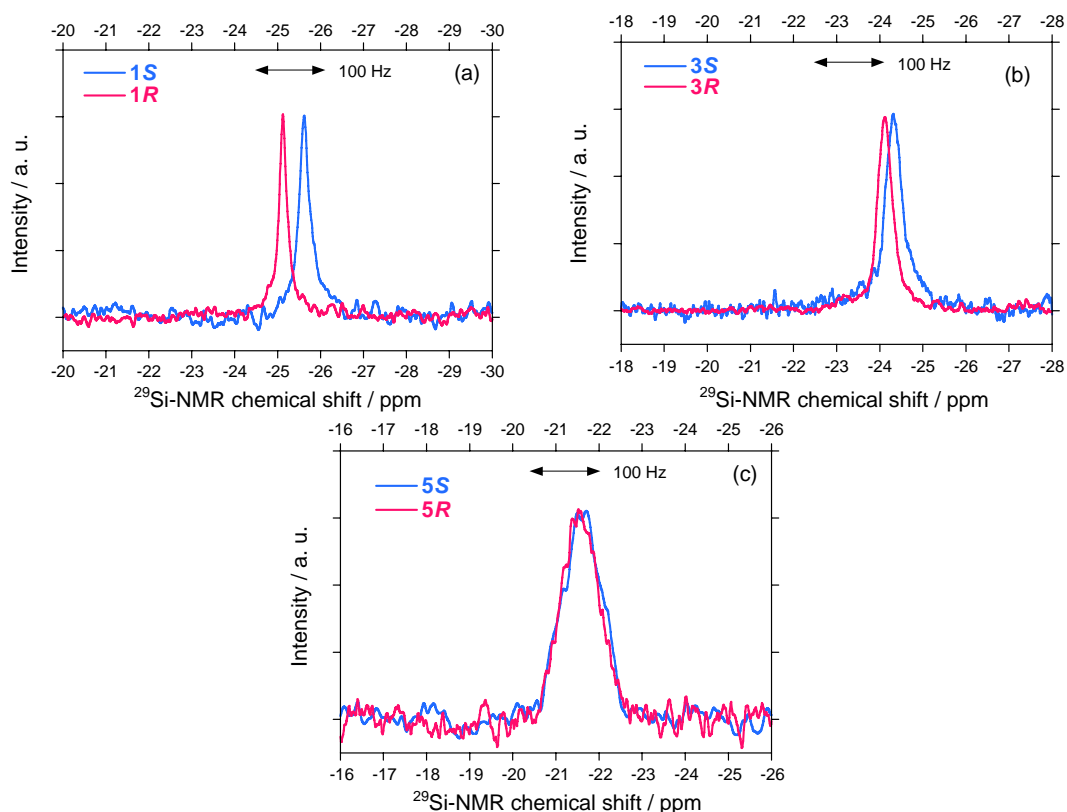
From the variable temperature CD/UV spectroscopic measurements and chiroptical analyses, three chiroptical parameters ($|g_{CD}|$, $|g_{PC}|$, and g_{PV}) of 1–6 are summarized in Table 1. Polysilanes 1–4 having helix-helix transition ability showed detectable differences in the $|g_{CD}|$ values in the range of -80°C to $+80^\circ\text{C}$, presumably, arising from considerable mixing of the g_{PV} and g_{PC} terms at any temperatures. Even polysilane **5**, which lacks the ability to transition, appears to mix g_{PV} with g_{PC} terms at -80°C . The signs of the g_{PV} values of **1–5** are negative, potentially, due to intrinsic physical origins and regardless of the side chain chiralities (chemical origins). The ratio of $|g_{PV}|$ to $|g_{PC}|$ ranges from 0.06 to 0.17. However, polysilane **6**, which lacks the ability to transition, did not markedly show this mixing in the range of -80°C to $+80^\circ\text{C}$. Possible reasons for these differences will be discussed in the following sections along with a relationship of the sign of the CD band and helix preference.

2.2. NMR Spectral Analysis

2.2.1. ^{29}Si -NMR Spectroscopic Features

A solution NMR spectrometer is commonly used in chemistry and biochemistry laboratories as a typical achiral physical detection system for observing nuclear spin states surrounded by multiple electrons. Considerable differences in the ^{29}Si -NMR spectral characteristics (chemical shift and linewidth) for helix-helix-transitioned **1S/1R** and **3S/3R** in CDCl_3 were detectable, as shown in Figures 9(a)–9(b). By contrast, very weak differences for the non-helix-helix-transitioned **5S/5R** pair were observed [Figure 9(c)].

Figure 9. ^{29}Si -NMR spectra of (a) **1S** ($M_w = 31,400$, $M_n = 17,400$) and **1R** ($M_w = 30,100$, $M_n = 20,000$) in CDCl_3 at $40\text{ }^\circ\text{C}$ (50 mg in CDCl_3 0.6 mL), (b) **3S** ($M_w = 44,000$ and $M_n = 31,100$) and **3R** ($M_w = 42,700$, $M_n = 29,000$) in CDCl_3 at $30\text{ }^\circ\text{C}$, and (c) **5S** ($M_w = 37,500$ and $M_n = 22,900$) and **5R** ($M_w = 28,700$, $M_n = 17,900$) in CDCl_3 at $30\text{ }^\circ\text{C}$.



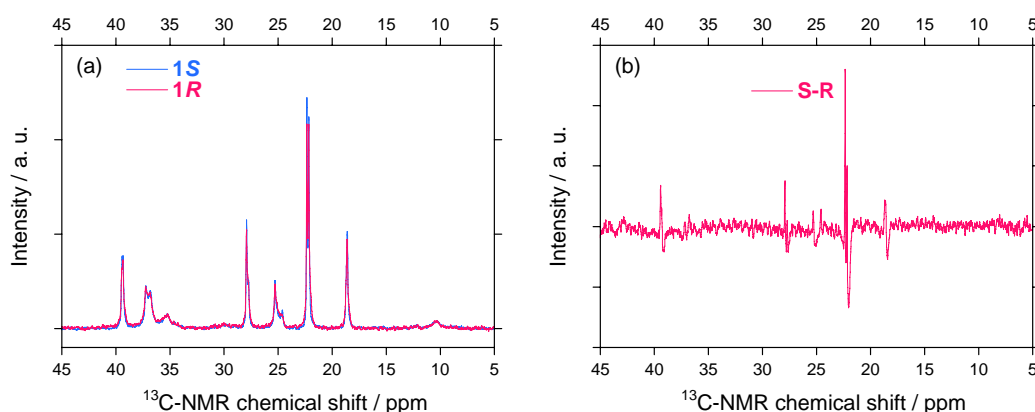
The ^{29}Si -NMR linewidths, which are a measure of the main chain mobility, of symmetrically substituted **1S/1R** are slightly different: **1S**: 19 Hz and **1R**: 13 Hz, suggesting that the main chain of **1S** is less mobile than its **1R** counterpart. A more clear difference is observed in the ^{29}Si -NMR chemical shifts: **1S** and **1R** resonances at -25.62 and -25.11 ppm, respectively, indicating that **1S** resonates by 31 Hz upfield of **1R**. Asymmetrically substituted **3S/3R** also gives subtle differences in the ^{29}Si -NMR chemical shifts and linewidths [Figure 9(b)]. Because **3S** and **3R** resonate at -24.30 and -24.11 ppm, respectively, **3S** resonates by 11.4 Hz upfield of **3R**. In addition, **3S** exhibit a broader linewidth ($\nu_{1/2} = 28$ Hz) than that of **3R** ($\nu_{1/2} = 24$ Hz).

The differences in ^{29}Si -NMR chemical shifts reach up to 10–30 Hz and therefore are possible to use for comparison with the theoretically predicted value of ~ 1 mHz for rotamers of H–El–El–H (El = O, S, Se, Te) containing heavier elements and other molecular systems [21,76,77]. One possible explanation for polysilane highpolymers is that the ^{29}Si -NMR chemical shift experiences an almost equal contribution in the opposite direction as a consequence of paramagnetic shielding (downfield shift) and diamagnetic shielding (upfield shift) tensors induced by electrons. By contrast, very weak differences in ^{29}Si -NMR for **5S** and **5R** at -21.6 ppm with a broader linewidth of ~ 72 Hz are observed even though **5S** had a ~ 5 Hz upfield resonance from that of **5R**. The difference could be related to the existence of the handed *WNC* governing the heavier helical Si–Si main chain dynamics.

2.2.2. ^{13}C -NMR Spectral Features

Subtle differences in ^{13}C -NMR spectral characteristics (chemical shifts and signal intensities) for **1S/1R** were observed [Figure 10(a)]. The ^{13}C -NMR signal intensities, which are a measure of side chain mobility, were slightly different between **1S** and **1R**. To numerically enhance the differences in the chemical shift and signal intensities, the difference spectrum between **1S** and **1R** was given in Figure 10(b). Several carbons of the (*S*)-side chain resonate at a downfield region compared to those of the (*R*)-side chain. A possible explanation is that the ^{13}C -NMR chemical shift experiences mainly as a consequence of paramagnetic shielding (downfield shift) tensors induced by electrons. This difference could infer the difference in dynamics of the side chain made of the lighter carbon atoms, influenced by the handed *WNC*.

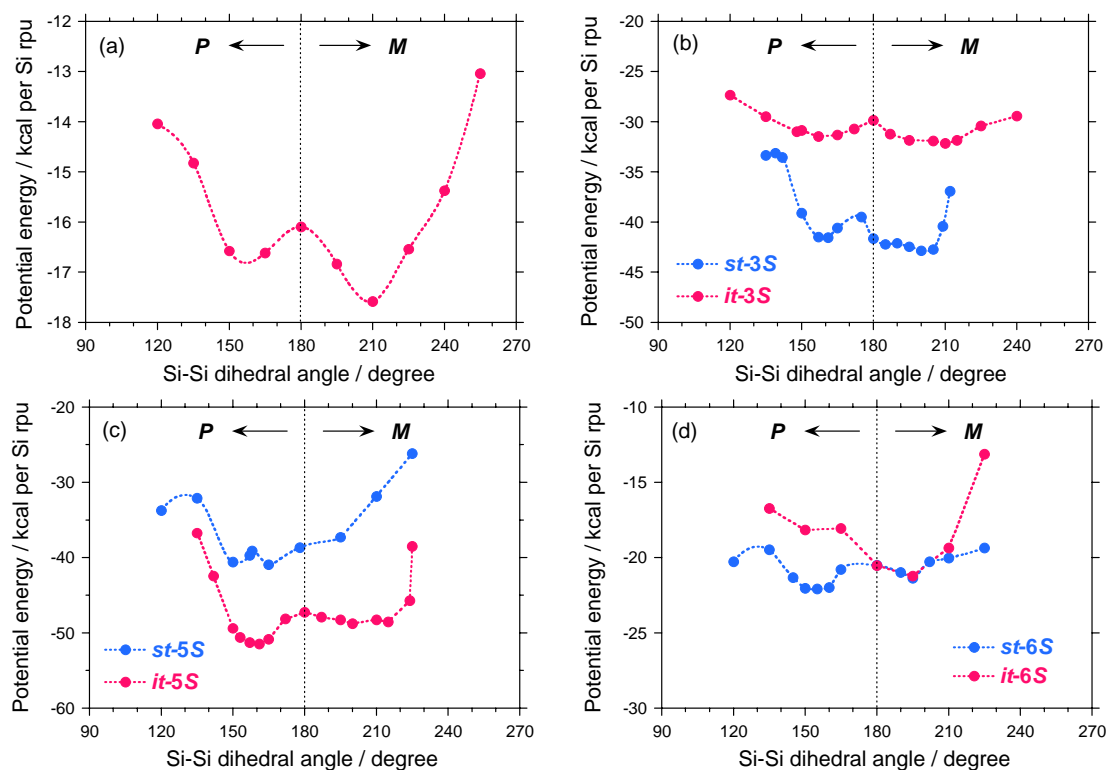
Figure 10. (a) ^{13}C -NMR spectra of **1S** ($M_w = 31,400$ and $M_n = 17,400$) and **1R** ($M_w = 30,100$, $M_n = 20,000$) in CDCl_3 at 40°C and (b) the difference spectrum between **1S** and **1R**.



2.3. Electronic Calculation and Molecular Mechanics Calculation

A possible explanation for the differences in the $|g_{\text{CD}}|$ values between the **1–4** pairs may be due to a slight modification of the potential energy surface as a function of the Si–Si–Si–Si dihedral angle of **1S**, isotactic (*it*) and syndiotactic (*st*) sequences of **3S**, as schematically shown in Figures 11(a)–11(b). For comparison, the potential energy surfaces of the *it*- and *st*-sequences of **5S** and **6S** are given in Figures 11(c)–11(d).

Figure 11. The potential energy of (a) **1S** with fifty Si-repeating units and hydrogen termini, (b) *st*- and *it*-**3S**s with thirty Si-repeating units and hydrogen termini, and (c) *st*- and *it*-**5S**s with thirty Si-repeating units and hydrogen termini, and (d) *st*- and *it*-**6S**s with *n*-hexyl-(*S*)-2-methylsilane with thirty Si-repeating units and hydrogen termini calculated for simplicity. Here *n*-hexyl moiety was used in place of *n*-dodecyl group for simplicity.



As shown in Figure 11(a), although **1S** has two local minima located at $\sim 150^\circ$ and $\sim 210^\circ$, it favors *M*-screw-sense as the global minimum. Dihedral angles of $\sim 150^\circ$ and $\sim 210^\circ$ correspond to 7_3 -helices with *P*- and *M*-screw-senses, respectively. The energy difference (ΔE) between the *P*- and *M*-helices is only ~ 1 kcal per Si-repeating unit and the E_B value from the *M*-helix is only ~ 2 kcal per Si-repeating unit. These small ΔE and E_B values are responsible for a thermo-driven helix-helix transition. Therefore, **1S** at -80°C preferentially adopts *M*-screw-sense, providing negative Cotton CD signals.

In the case of **3S**, due to asymmetrically substituted side groups, the *it*- and *st*-sequences should be considered. Although both the *it*- and *st*-sequences have two local minima located at $\sim 150^\circ$ and $\sim 210^\circ$, they slightly favor *M*-screw-sense as the global minimum. With global minima between *it*- and *st*-sequences, the *st*-sequence with *M*-screw-sense is the most stable of the four possible helices. Therefore, *M-st-3S* is assumed to be the global minimum. The value of ΔE between the *P*- and *M*-helices is only ~ 1 kcal per Si-repeating unit and the E_B value of *M*-helix is only ~ 3 kcal per Si-repeating unit. Similar to **1S**, the small ΔE and E_B values of *M-st-3S* are responsible for the thermo-driven helix-helix transition. Therefore, **3S** at -80°C preferentially adopts *M*-screw-sense, providing the negative CD signal.

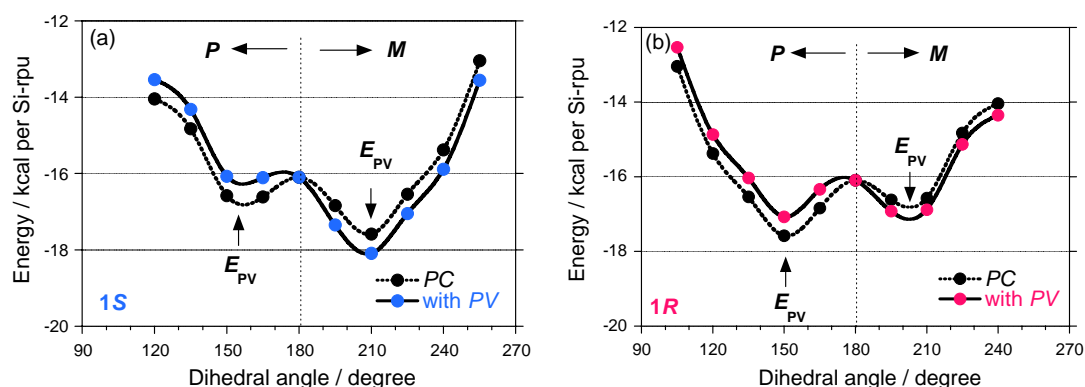
In case of **5S**, the *st*-sequence has a single minimum located at $\sim 195^\circ$, while the *it*-sequence has two local minima located at $\sim 150^\circ$ and $\sim 195^\circ$. Among the three minima, the *it*-sequence with *P*-screw-sense

may be a global minimum, suggesting that **5S** at $-80\text{ }^{\circ}\text{C}$ may prefer *P*-screw-sense, thereby yielding a positive CD signal.

When the relationship between the CD sign and *P*-/*M*-preference for **1**, **3**, and **5** with the *S*-chiral group was compared, the helix-helix transition polysilanes carrying the *S*-chiral group favor *M*-screw-sense, thus exhibiting a negative CD band. Conversely, the non-helix-helix transition polysilane carrying the same *S*-chiral group favors *P*-screw-sense and exhibits a positive CD band. These ideas are consistent with the experimental results [Figures 4(a), 7(a)–7(c), and 8(a)].

The potential energy curves for models of **1S** and **1R** with fifty Si repeating units with uncorrected and corrected *PV* terms are schematically shown in Figure 12. Although commercial molecular mechanics packages do not include any parity violation effects and high level *ab initio* techniques using the *PV* Hamiltonian is needed in future, the small positive E_{PV} bias of $+0.5\text{ kcal}$ for the *P*-motif and a small negative E_{PV} of -0.5 kcal for the *M*-motif were added for explanation purpose only, regardless of the side chain chirality in which helix induction is governed by the *PC* electromagnetic force origin. Note that these values are not exact and merely *hypothetically*.

Figure 12. The potential energy of (a) **1S** and (b) **1R** with hypothetical corrections of E_{PV} of $+0.5\text{ kcal}$ for *P*- and -0.5 kcal for *M*-screw-senses for explanation purpose only.



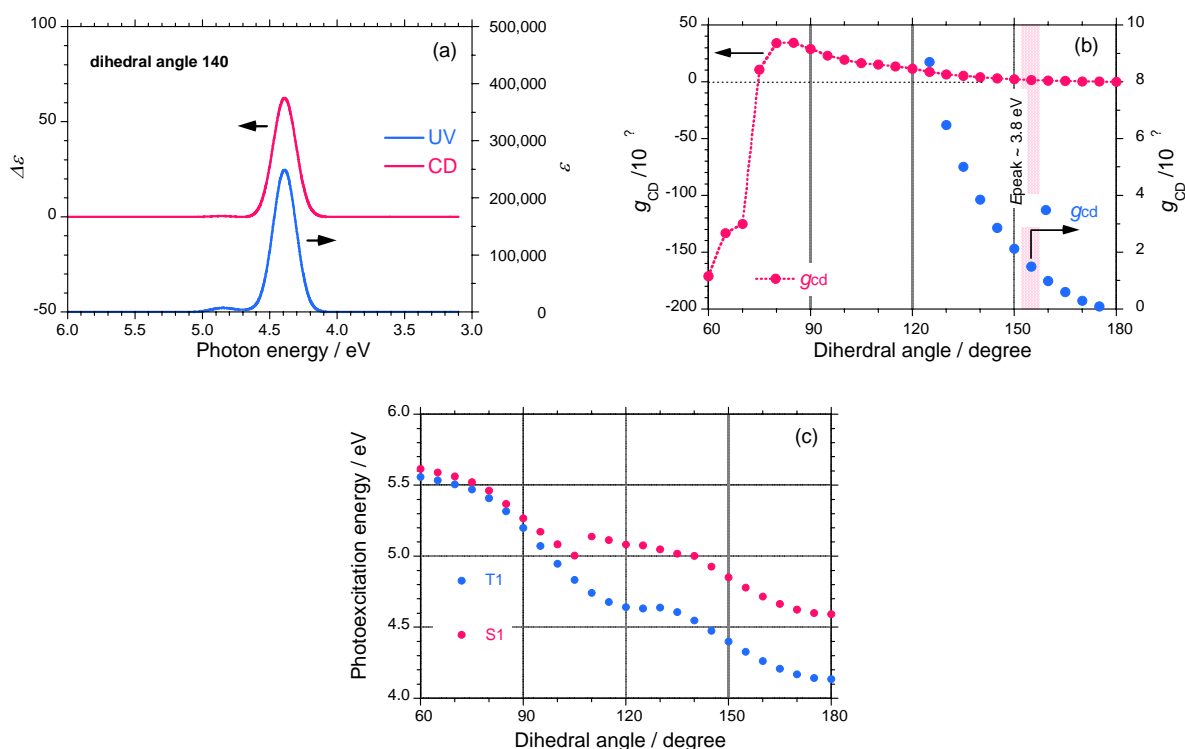
Before the *PV* term addition, **1S** and **1R** were classified into classical mirror images of helical polymers because of an almost degenerate asymmetric double well. If the E_{PV} bias effectively allow for the induction of inequality to the potential energy by $\exp(2 \cdot E_{PV}/kT)$, the double-well potential curves do not keep the mirror image relationship. In the images and mirror images of helical polymers **1–5**, the absolute g_{CD} values of the negative CD signals at $-80\text{ }^{\circ}\text{C}$, possibly due to their *M*-screw-sense preference, are greater than those for the corresponding *P*-one, regardless of the side chain chirality and temperature. These observations suggest that the sign of g_{PV} may be negative for the **1–5** pairs and that their preferential screw-sense is *M* rather than *P* because the *P*-helix should give a positive CD signal.

In the case of **6S** carrying an (*S*)-2-methylbutyl moiety, the *it*-sequence has a single minimum located at $\sim 195^{\circ}$, while the *st*-sequence has two local minima located at $\sim 150^{\circ}$ and $\sim 195^{\circ}$. Among the three minima, the *P-st*-sequence may be a global minimum, suggesting that **6S** at $-80\text{ }^{\circ}\text{C}$ may preferentially adopt a *P*-screw-sense, thus yielding positive CD signals, which are consistent with the experimental results [Figure 8(b)].

From these molecular mechanics calculations, the potential energy in the almost degenerate double well with small ΔE and E_B values is responsible for the thermo-driven helix–helix transition ability due

to the flexible helical main chain. These features are assumed to be important for detecting subtle differences by the *PV*-force origin for helical polymers. By contrast, the potential energy in the almost single well with the large ΔE and E_B values cannot afford the subtle differences due to a very rigid helical structure. The helical main chain flexibility in a double well with small ΔE and E_B values, leading to quantum tunneling oscillation, is important for testing the *MPV* hypothesis.

Figure 13. (a) Simulated UV and CD spectra of $(\text{SiH}_2)_{13}$ with a dihedral angle of P -140°, (b) simulated g_{CD} as a function of the dihedral angle in $\text{H}-(\text{SiH}_2)_{13}-\text{H}$, (c) photoexcitation energies (singlet and triplet states) of $\text{H}-(\text{SiH}_2)_{13}-\text{H}$ as a function of the dihedral angle.



To further confirm the relationship between the screw-sense, absolute magnitude of g_{CD} , and CD sign, Gaussian03 calculations (TD-DFT, B3LYP, 3-21G basis set) of the parent oligosilane, $\text{H}-(\text{SiH}_2)_{13}-\text{H}$, as a model of a polysilane were performed [78]. The simulated UV and CD spectra of oligosilane with a dihedral angle of 140° are shown in Figure 13(a). The spectral shape of the CD signals completely matches the corresponding UV spectrum, which is distinct for helical polysilanes. Based on the spectral characteristics, the g_{CD} values of the parent polysilane monotonically increase from zero to $+8 \times 10^{-4}$ as the dihedral angle changes from 180° to 125° [Figure 13(b)]. The g_{CD} values change the sign from positive to negative at a dihedral angle of less than $\sim 75^\circ$ and the absolute magnitude markedly increases to -1.7×10^{-2} as the dihedral angle changes from 100° to 60°.

When the dihedral angle changes from 180° to 60°, the electrically allowed transition energy between the singlet-singlet (S_0-S_1) states monotonically increases from 4.6 eV to 5.6 eV. Similarly, the electrically forbidden transition energy between the singlet-triplet (S_0-T_1) states, though the oscillator strength is zero, monotonically increases from 4.2 eV to 5.5 eV (Figure 12(c)). The g_{CD} value of a 7_3 -helix with a dihedral angle of 155° was calculated to be $+1.4 \times 10^{-4}$, which is in good agreement with

the observed g_{CD} values of $\sim 2.5 \times 10^{-4}$ for **5** and **6** bearing (*S*)-chiral side groups. The molecular mechanics and Gaussian calculations suggest that the *P*-screw-sense of polysilane gives a positive CD band when the dihedral angle is between 75° and 180° .

2.4. Viscometric Measurements

Slight differences were also observed in the viscometric data (κ and α) in the Kuhn-Mark-Houwink-Sakurada plots ($[\eta] = \kappa \cdot M^\alpha$ [79], where $[\eta]$ is intrinsic viscosity, M is molecular weight, κ is a constant, and α is viscosity index) between the four pairs of **1**, **2**, **3**, **5**, and **6** in chloroform at 30°C , in tetrahydrofuran (THF) at 40°C , and in toluene at 70°C . The viscometric measurement is well-established as a physico-chemical method to characterize floppy chain-like polymers in dilute solution. Based on the *MPV* hypothesis, the degree of chain coiling mediated by handed inner-shell electrons interacting with the massive nucleus may result in subtle differences in the value of α over a wide range of molecular masses between the polysilane pairs.

According to measurements and analyses by TRC and the NTT R&D center [1996/03/06 (report no. T113613), 1998/09/25 (report no. T215754), 1999/03/05 (report no. T218558), 1999/05/19 (report no. T218904)], subtle differences in the α values of the unfractionated polymer samples were observed experimentally. These features could be associated with differences in the main chain stiffness of the polysilane pairs in solution: for **1** (chloroform at 30°C), **1S**, $\alpha = 1.13$, **1R**, $\alpha = 1.26$; for **1** (toluene, 70°C), **1S**, $\alpha = 1.70$, **1R**, $\alpha = 1.57$; for **2** (THF, 30°C), **2S**, $\alpha = 0.91$, **2R**, $\alpha = 0.97$; for **3** (toluene, 70°C), **3S**, $\alpha = 1.47$, **3R**, $\alpha = 1.32$; for **3** (THF, 30°C), **3S**, $\alpha = 1.47$, **3R**, $\alpha = 1.32$; for **5** (toluene, 70°C), **5S**, $\alpha = 1.49$, **5R**, $\alpha = 1.36$; for **5** (THF, 30°C), **5S**, $\alpha = 1.29$, **5R**, $\alpha = 1.22$; for **6** (toluene, 70°C), **6S**, $\alpha = 1.21$, **6R**, $\alpha = 1.49$; for **6** (THF, 30°C), **6S**, $\alpha = 0.93$, **6R**, $\alpha = 0.88$.

3. Experimental Section

3.1. Measurements

All CD and UV absorption spectra were recorded simultaneously on a JASCO J-720 spectropolarimeter equipped with a liquid nitrogen-controlled quartz cell with a path length of 5 mm in a cryostat ranging from $+23^\circ\text{C}$ to -90°C and a Peltier-controlled quartz cell with a path length of 10 mm ranging from $+90^\circ\text{C}$ to -10°C . This temperature range assured that isooctane was sufficiently fluid because the melting and boiling points of isooctane are -100°C and $+100^\circ\text{C}$, respectively. The scanning conditions were as follows: scanning rate of 50 nm per min, band width of 1 nm, response time of 1 sec, and twice or single accumulations. The solution temperature in the cryostat was monitored by directly immersing a thermocouple into the solution, while the solution temperature in the Peltier-controlled cell was considered to be the same as the aluminum block cell housing. The sample concentration was 2×10^{-5} (Si-repeat-unit) $^{-1} \cdot \text{dm}^{-3}$ for UV and CD measurements. The ^{13}C - (75.43 MHz) and ^{29}Si - (59.59 MHz) NMR spectra were taken in CDCl_3 at 30°C or 40°C with a Varian Unity 300 MHz NMR spectrometer using tetramethylsilane as an internal standard. Optical rotation at the Na-D line was measured with a JASCO DIP-370 polarimeter using a synthetic quartz (SQ) cell with a path length of 10 mm at room temperature (24°C). The weight-average molecular weight (M_w) and number-average molecular weight of the polymers (M_n) were evaluated using gel permeation chromatography (Shimadzu A10 instruments,

Shodex KF-806M column, and HPLC-grade tetrahydrofuran as eluent at 30 °C) based on calibration with polystyrene standards (Tohso). The intrinsic viscosity–molecular weight relationship was investigated at the Toray Research Center (TRC, Shiga, Japan) using a Waters 1500 GPC apparatus with a Viscotec H502a viscometer.

3.2. Monomer Synthesis

The Toray Research Center (TRC) and Nippon Telegraph and Telephone Corporation (NTT) R&D center [reported on 1998/03/11 (report no. T216669), 1998/06/29 (report no. T217117), 1998/08/17 (report no. T217601)] analyzed the enantiopurities of the starting materials and intermediates. These materials were used to prepare chiral organodichlorosilanes as follows (in %*ee*) by a Grignard coupling reaction of the corresponding alkylbromide with alkyltrichlorosilanes by means of a chiral GC technique (β -DEX225 and β -DEX325, Spelco): (*S*)-(+)-/(*R*)-(–)-citronellol = 97.4/97.9, (*S*)-(+)- β /(*R*)-(–)- β -citronellol = 97.4/97.9, (*S*)-(–)-/(*R*)-(+)-3,7-dimethyloctanol = 95.9/95.7, (*S*)-(–)-/(*R*)-(+)-3,7-dimethylbromide = 95.0/96.6, (*S*)-(–)-/(*R*)-(+)-2-methylbutanol = 99.7/100.0. (See, Appendix, Figure A3 and A4).

A typical synthetic scheme of **1S** and **1R** is given in the Appendix, Scheme A1. The Grignard reagent obtained from 41.3 g (0.186 mol) of (*R*)-(–)-3,7-dimethyloctylbromide ($[\alpha]_D^{24} = -5.96^\circ$ (neat), 96.0 %*ee*) was added to a solution of 13.3 g (7.82 mmol) of tetrachlorosilane (Shin-Etsu) in dry diethylether at room temperature to produce *bis*{(*R*)-(–)-3,7-dimethyloctyl}dichlorosilane. The bromide was prepared at Chemical Soft (Kyoto, Japan) by bromination of (*R*)-(+)-3,7-dimethyloctanol ($[\alpha]_D^{24} = +3.90^\circ$ (neat), 95.7 % *ee*) with PPh₃ and Br₂ in CCl₄, followed by hydrogenation of (*R*)-(*d*)-(+)- β -citronellol (Fluka, $[\alpha]_D^{24} = +4.46^\circ$ (neat), 97.9 % *ee*). Filtration of the reaction mixture and vacuum distillation of the filtrate produced pure alcohol. Colorless liquid. Yield 11.0 g (37 %). bp 142–146 °C/0.18 Torr, $[\alpha]_D^{24} = -2.57^\circ$ (neat), ²⁹Si-NMR (CDCl₃, 30 °C, ppm) 34.75, ¹³C-NMR (CDCl₃, 30 °C, ppm) 17.36, 19.10, 22.62, 22.71, 24.74, 27.96, 29.13, 34.79, 36.46, 39.30.

Bis{(*S*)-(+)-3,7-dimethyloctyl}dichlorosilane} was synthesized in a similar way using (*S*)-(+)-3,7-dimethyloctylbromide ($[\alpha]_D^{24} = +6.05^\circ$ (neat), 96.2 %*ee*, Chemical Soft) from (*S*)-(–)-3,7-dimethyloctanol ($[\alpha]_D^{24} = -4.22^\circ$ (neat), 95.9 %*ee*) and (*S*)-(*l*)-(–)- β -citronellol (Fluka, $[\alpha]_D^{24} = -4.55^\circ$ (neat), 97.4 %*ee*) as the starting material. Colorless liquid. bp 142–144 °C/0.52 Torr, $[\alpha]_D^{24} = +2.35^\circ$ (neat), ²⁹Si-NMR (CDCl₃, 30 °C, ppm) 34.74, ¹³C-NMR (CDCl₃, 30 °C, ppm) 17.35, 19.10, 22.62, 22.71, 24.73, 27.96, 29.13, 34.79, 36.45, 39.29.

The enantiopurity of the starting materials and intermediates was determined at TRC by chiral gas chromatography (Spelco, β -DEX-325 and β -DEX-225, 30 m × 0.25 mm ID, oven temperature of 70 °C–95 °C, He carrier with 1.2 mL/min; β -DEX-225 at 90 °C for citronellol, β -DEX-225 at 82 °C for 3,7-dimethyloctanol, and β -DEX-325 at 70 °C for 3,7-dimethylbromide). The author concluded that the image and mirror image starting materials and intermediates and the corresponding organodichlorosilanes had sufficiently high enantiopurity with almost identical *ees*. However, the chiral GC analysis at TRC indicated that the enantiopurity of (*S*)-(*l*)-(–)- β -3,7-citronellol (Merck, $[\alpha]_D^{24} = -3.11^\circ$ (neat)) was only 64.8 %*ee* and of (*S*)-(–)-3,7-dimethyloctanol (Chemical Soft, using Merck's product, (*S*)-(*l*)-(–)- β -3,7-citronellol) was 66.4 %*ee*. Therefore, the author used Fluka products as starting materials for the TRC analysis.

(*R*)-(-)-3,7-dimethyloctyl-2-methylpropyldichlorosilane, bp 86–92 °C/0.45 Torr, $[\alpha]_D^{24} = -1.77^\circ$ (neat), $^{29}\text{Si-NMR}$ (CDCl_3 , 30 °C, ppm) 33.21, $^{13}\text{C-NMR}$ (CDCl_3 , 30 °C, ppm) 18.37, 19.04, 22.56, 22.66, 24.14, 24.67, 25.55, 27.91, 29.10, 30.25, 34.73, 36.40, 39.24.

(*S*)-(+)-3,7-dimethyloctyl-2-methylpropyldichlorosilane, bp 89–93 °C/0.60 Torr, $[\alpha]_D^{24} = +1.81^\circ$ (neat), $^{29}\text{Si-NMR}$ (CDCl_3 , 30 °C, ppm) 33.34, $^{13}\text{C-NMR}$ (CDCl_3 , 30 °C, ppm) 18.43, 19.09, 22.61, 22.70, 24.20, 24.72, 25.60, 27.96, 29.16, 30.31, 34.78, 36.45, 39.29.

(*R*)-(-)-3,7-dimethyloctyl-3-methylbutyldichlorosilane, bp 104–105 °C/0.50 Torr, $[\alpha]_D^{24} = -1.61^\circ$ (neat), $^{29}\text{Si-NMR}$ (CDCl_3 , 30 °C, ppm) 34.65, $^{13}\text{C-NMR}$ (CDCl_3 , 30 °C, ppm) 17.36, 17.89, 19.11, 21.98, 22.63, 22.72, 24.74, 27.98, 29.12, 30.18, 31.16, 34.79, 36.47, 39.31.

(*S*)-(+)-3,7-dimethyloctyl-3-methylbutyldichlorosilane, bp 122–127 °C/1.5 Torr, $[\alpha]_D^{24} = +1.61^\circ$ (neat), $^{29}\text{Si-NMR}$ (CDCl_3 , 30 °C, ppm) 34.67, $^{13}\text{C-NMR}$ (CDCl_3 , 30 °C, ppm) 17.35, 17.88, 19.10, 21.97, 22.62, 22.71, 24.73, 27.97, 29.12, 30.17, 31.15, 34.78, 36.46, 39.30.

(*R*)-(-)-3,7-dimethyloctyl-3-cyclopentylethyldichlorosilane, bp 131–133 °C/0.80 Torr, $[\alpha]_D^{24} = +1.40^\circ$ (neat), $^{29}\text{Si-NMR}$ (CDCl_3 , 30 °C, ppm) 34.27, $^{13}\text{C-NMR}$ (CDCl_3 , 30 °C, ppm) 17.38, 19.11, 19.36, 22.63, 22.71, 24.74, 25.25, 27.98, 28.52, 29.12, 32.26, 34.79, 36.46, 39.31, 42.42.

(*S*)-(+)-3,7-dimethyloctyl-3-cyclopentylethyldichlorosilane, bp 115–118 °C/0.35 Torr, $[\alpha]_D^{24} = +1.52^\circ$ (neat), $^{29}\text{Si-NMR}$ (CDCl_3 , 30 °C, ppm) 34.31, $^{13}\text{C-NMR}$ (CDCl_3 , 30 °C, ppm) 17.38, 19.10, 19.34, 22.62, 22.70, 24.73, 25.24, 27.97, 28.51, 29.11, 32.25, 34.78, 36.45, 39.29, 42.41.

(*R*)-(-)-3,7-dimethyloctyl-2-ethylbutyldichlorosilane, bp 80–81 °C/0.55 Torr, $[\alpha]_D^{24} = -1.63^\circ$ (neat), $^{29}\text{Si-NMR}$ (CDCl_3 , 30 °C, ppm) 34.23, $^{13}\text{C-NMR}$ (CDCl_3 , 30 °C, ppm) 10.56, 18.42, 19.11, 22.63, 22.71, 24.69, 24.76, 27.75, 27.99, 29.23, 34.83, 35.97, 36.51, 39.33.

(*S*)-(+)-3,7-dimethyloctyl-2-ethylbutyldichlorosilane, bp 123–124 °C/2.2 Torr, $[\alpha]_D^{24} = +1.73^\circ$ (neat), $^{29}\text{Si-NMR}$ (CDCl_3 , 30 °C, ppm) 34.15, $^{13}\text{C-NMR}$ (CDCl_3 , 30 °C, ppm) 10.50, 18.36, 19.06, 22.57, 22.66, 24.62, 24.70, 27.69, 27.93, 29.17, 34.76, 35.90, 36.44, 39.26.

(*R*)-(+)-2-methylbutyl-*n*-dodecyldichlorosilane, bp 128–135 °C/0.60 Torr, $[\alpha]_D^{24} = -6.22^\circ$ (neat), $^{29}\text{Si-NMR}$ (CDCl_3 , 30 °C, ppm) 33.18, $^{13}\text{C-NMR}$ (CDCl_3 , 30 °C, ppm) 11.21, 14.11, 21.35, 21.85, 22.47, 22.72, 28.15, 29.15, 29.38, 29.48, 29.67, 30.27, 31.96, 32.38, 32.52.

(*S*)-(+)-2-methylbutyl-*n*-dodecyldichlorosilane, bp 148–151 °C/0.35 Torr, $[\alpha]_D^{24} = +6.27^\circ$ (neat), $^{29}\text{Si-NMR}$ (CDCl_3 , 30 °C, ppm) 33.18, $^{13}\text{C-NMR}$ (CDCl_3 , 30 °C, ppm) 11.23, 14.14, 21.33, 21.84, 22.45, 22.72, 28.08, 29.15, 29.39, 29.48, 29.37, 30.24, 31.95, 32.37, 32.52.

3.3. Polymer Preparation

A typical synthetic procedure is described for **1S** as follows. To a mixture of 12 mL of dry toluene (Kanto), 0.75 g (33 mmol) of sodium (Wako), and 0.06 g (0.23 mmol) of 18-crown-6 (Wako), 4.0 g (11 mmol) of diorganodichlorosilane was added dropwise in an argon atmosphere. The mixture was stirred slowly at 110 °C. After 3 hours, 200 mL of dry toluene was added to reduce the solution viscosity, and the mixture was stirred continuously for an additional 30 minutes. The hot reaction mixture slurry was passed immediately through a 5- μ m PTFE filter under argon gas pressure. To the clear filtrate, the precipitating solvents isopropanol and ethanol were carefully added. Several portions of the white precipitates were collected by centrifugation and dried at 120 °C under vacuum overnight.

The weight-average molecular weight (M_w) and number-average molecular weight (M_n) of the polymers were evaluated using gel permeation chromatography (Shimadzu A10 instrument, Shodex KF806M column, and HPLC-grade tetrahydrofuran as eluent at 30 °C), based on calibration with polystyrene standards as follows. For the purpose of chiroptical measurements, **1S**, $M_w = 863,000$, $M_n = 147,000$ and $M_w = 140,000$, $M_n = 34,400$; **1R**, $M_w = 394,000$, $M_n = 85,800$ and $M_w = 149,000$, $M_n = 39,500$; **2S**, $M_w = 93,100$, $M_n = 57,900$; **2R**, $M_w = 51,800$, $M_n = 25,200$, **3S**, $M_w = 232,000$, $M_n = 78,900$; **3R**, $M_w = 156,000$, $M_n = 76,800$, **4S**, $M_w = 14,500$, $M_n = 11,300$; **4R**, $M_w = 19,000$, $M_n = 15,200$, **5S**, $M_w = 42,300$, $M_n = 23,500$; **5R**, $M_w = 36,900$, $M_n = 19,000$, **6S**, $M_w = 108,000$, $M_n = 37,300$; **6R**, $M_w = 80,900$, $M_n = 34,600$.

For NMR measurements, lower molecular mass samples with an almost equal M_w value were used: **1S**, $M_w = 31,400$ and $M_n = 17,400$; **1R**, $M_w = 30,100$, $M_n = 20,000$; **3S**, $M_w = 44,000$ and $M_n = 31,100$; **3R**, $M_w = 42,700$, $M_n = 29,000$; **5S**, $M_w = 37,500$ and $M_n = 22,900$; **5R**, $M_w = 28,700$, $M_n = 17,900$.

3.4. Molecular Mechanics Calculations

Molecular mechanics calculations were achieved using Molecular Simulation Inc. (MSI), the Discover 3 module, Ver. 4.00 on a Silicon Graphics Indigo II XZ computer based on standard parameters (default) with an Si-Si bond length of 2.34 Å, an Si-Si-Si bond angle of 111°, and the MSI pcff force field suitable for polymers. For this calculation, the MSI built-in functions of simple-minimize (default condition is dihedral angle restraints, steepest descents for the first derivative, iteration limit of 1000, movement limit of 0.2, and derivative for 1.0) and simple-dynamics (conditions of constant volume and temperature, initial temperature of 300 K, direct velocity scaling with a time step of 1 fs, integration, initial velocity of random velocities from the Boltzmann distribution) were used with the set-up parameters.

3.5. Electronic State Calculation using Gaussian03 [78]

Electronic state calculations including the parent polysilane, H-(HSiH₂)₁₃-H, as a model of the present polysilanes, was employed using the time-dependent (TD)-density function DFT Gaussian03 program (TD-DFT, B3LYP, 3-21G basis sets) running on an Apple iMac (IntelCoreDuo2, 2.0 GHz, 4GB memory, MacOS ver.10.4.11). For the calculations, the geometries of the parent polysilane with dihedral angles varying from 80° to 180° with 5° and 10° intervals were optimized by the PM3-MM level of Gaussian03 using initial standard parameters (default) with an Si-Si bond length of 2.34 Å and an Si-Si-Si bond angle of 111°.

4. Conclusions

The experimental data in the absolutely artificial helical polysilanes may *not* provide conclusive proof to support the *MPV* hypothesis and the inherent physical origin of homochirality on Earth. Subtle differences in enantiopurity, tacticity, molecular weight, and molecular weight distribution of the polysilanes used in this work may have affected the chiroptical properties and the achiral NMR (^{29}Si and ^{13}C) as well as achiral viscometric data. Nevertheless, the author believed that the differences demonstrated here may infer the emergence of a preference between left and right at the polysilane level in isotropic solutions by certain inherent physical origins such as *WNC*, though the present experiments do not unequivocally support the *MPV* hypothesis. The subtle left-right asymmetry may appear in four pairs of helix-helix transition polysilanes (**1–4**), whereas two pairs of non-helix-helix transition polysilanes (**5**, **6**) are not evident. If the *MPV* hypothesis is correct, a real enantiomer of the helical polysilane with *M*-screw-sense may be an anti-polysilane with *M*-screw-sense made of anti-atoms, which is possible to exist in the anti-matter world [18,23,24,31], in the framework of the *CPT* conservation theorem by the indication of recent *CP*-symmetry breaking of the *B*-meson decay experiments and theory [80–82].

5. Acknowledgements

The major part of the present work was carried out from 1995 to 2001 when the author worked for NTT Basic Research Laboratory where Hiromi Tamoto–Takigawa (worked for NTT-AT) and Masao Motonaga (worked for CREST-JST) measured and analyzed the variable temperature UV/CD spectra of the polysilanes in solution. The author synthesized the polysilanes and characterized by NMR and GPC. The potential energy surface (MSI, Discover 3) and electronic state (Gaussian03) were calculated at NTT (FY 1998–FY2000) and NAIST (FY 2009), respectively.

The author gratefully acknowledges Profs. Julian R. Koe (International Christian University (International Christian University)), Kyozauro Takeda (Waseda University), Hiroyuki Teramae (Jousei University), Nobuo Matsumoto (Shonan Institute of University), Masaie Fujino (Gunma National College of Technology), Kazuaki Furukawa (NTT), Takahiro Sato (Osaka University), Noriyuki Hatakenaka (Hiroshima University), the late Akio Teramoto (Osaka University, Emeritus), Masaki Hasegawa (University of Tokyo, Emeritus), Hideki Sakurai (Tohoku University, Emeritus), Toyoki Kunitake (Kyushu University, Emeritus), Junji Watanabe (Tokyo Institute of Technology), Kento Okoshi (Tokyo Institute of Technology), Masashi Kunitake (Kumamoto University), Zhang-Biao Zhang (Tianjin Normal University), Yong-Gang Yang (Soochow University), Eiji Yashima (Nagoya University), Yoshihisa Inoue (Osaka University), Hiroshi Masuhara (NAIST), Teruki Sugiyama (NAIST), Yoshio Okamoto (Nagoya University, Emeritus), Kenso Soai (Tokyo Science of University), and Wei Zhang (Soochow University) for their intuitive insights on helical polysilanes, entropy driven transitions, and chiroptical analysis from the early stage of this work until now. MF is also thankful to Drs. Hiroshi Nakashima (NTT), Osamu Niwa (AIST), Hong-Zhi Tang (Afton Chemicals), Anubhav Saxena (Momentive), Roopali Rai (Momentive), Akihiro Ohira (AIST), Masaaki Ishikawa (JASCO), Takayoshi Kawasaki (Tokyo Institute of Technology), Kenji Gomi (Kodansha Scientific), Masao Morita (NTT-AT), Masanobu Naito (NAIST), and Hisanari Onouchi (Nitto Denko) for fruitful discussions. The

author wishes to thank his students at NAIST, Yoshihiro Kimura, Fumiko Ichiyanagi, Dr. Yoko Nakano (Eindhoven University of Technology), Takashi Mori, Satoshi Fukao, Jalilah Binti Abd Jalil, Yoshifumi Kawagoe, Ayako Nakao, and Makoto Taguchi for stimulating discussions. The author is grateful for fund from CREST-JST (FY1998–FY2003), Grant-in-Aid for Scientific Research for Exploratory Research from MEXT (16655046, FY2004–FY2006), the NAIST Foundation (FY2009), the SEKISUI Chemical Grant Program for Research on Manufacturing Based on Learning from Nature (FY2010), and Grant-in-Aid for Scientific Research (B) from MEXT (22350052, FY2010–FY2013). The author is particularly grateful to Profs. Martin Quack (ETH), Robert Compton (University of Tennessee), Robert West (University of Wisconsin), Leo W. Jenneskens (University of Utrecht), and Victor Borovkov (Osaka University) for stimulating discussions at international symposiums and domestic conferences. Finally, the author acknowledges Prof. David B. Cline (University of California, LA) for giving the author an opportunity to describe this unpublished work in the special issue of Symmetry of Life and Homochirality.

6. References

1. Kipping, F.S.; Pope, W.J. Enantiomorphism. *J. Chem. Soc.* **1898**, *73*, 606–617.
2. Frank, F.C. On spontaneous asymmetric synthesis. *Biochim. Biophys. Acta* **1953**, *11*, 459–463.
3. Wald, G. The origin of optical activity. *Ann. N.Y. Acad. Sci.* **1957**, *69*, 352–368.
4. Ulbricht, T.L.V.; Vester, F. Attempts to induce optical activity with polarized β -radiation. *Tetrahedron* **1962**, *18*, 629–637.
5. Yamagata, Y. A hypothesis for the asymmetric appearance of biomolecules on Earth. *J. Theoret. Biol.* **1966**, *11*, 495–498.
6. Thiemann, W.; Darge, W. Experimental attempts for the study of the origin of optical activity on earth. *Orig. Life* **1974**, *5*, 263–283.
7. Rein, D. Some remarks on parity violating effects of intramolecular interactions. *J. Mol. Evol.* **1974**, *4*, 15–22.
8. Letokhov, V.S. On difference of energy levels of left and right molecules due to weak interactions. *Phys. Lett.* **1975**, *53A*, 275–276.
9. Zel'dovich, B.Ya.; Saakyan, D.B.; Sobel'man, I.I. Energy difference between right- and left-hand molecules, due to parity nonconservation in weak interactions of electrons with nuclei. *Sov. Phys. JETP. Lett.* **1977**, *25*, 94–97.
10. Keszthelyi, L. Origin of the asymmetry of biomolecules and weak interaction. *Orig. Life* **1977**, *8*, 299–340.
11. Harris, R.A.; Stodolsky, L. Quantum beats in optical activity and weak interactions. *Phys. Lett.* **1978**, *78B*, 313–317.
12. Hegstrom, R.A.; Rein, D.W.; Sandars, P.G.H. Calculation of the parity nonconserving energy difference between mirror-image molecules. *J. Chem. Phys.* **1980**, *73*, 2329–2341.
13. Mason, S.F. Origins of biomolecular handedness. *Nature* **1984**, *311*, 19–23.
14. Hegstrom, R.A. Weak neutral current and β radiolysis effects on the origin of the biomolecular chirality. *Nature* **1985**, *315*, 749–750.

15. Kondepudi, D.K.; Nelson, G.W. Weak neutral currents and the origin of biomolecular chirality. *Nature* **1985**, *314*, 438–441.
16. Mason, S.F.; Tranter, G.E. The electroweak origin of biomolecular handedness. *Proc. R. Soc. Lond.* **1985**, *A397*, 45–65.
17. Quack, M. On the measurement of the parity violating energy difference between enantiomers. *Chem. Phys. Lett.* **1986**, *132*, 147–153.
18. Barron, L.D. Symmetry and molecular chirality. *Chem. Soc. Rev.* **1986**, *15*, 189–223.
19. Applequist, J. Optical activity: Biot's bequest. *Amer. Sci.* **1987**, *75*, 59–68.
20. Wiesenfeld, L. Effect of atomic number on parity-violating energy differences between enantiomers, O, S, Se, Te. *Mol. Phys.* **1988**, *64*, 739–745.
21. Barra, A.L.; Robert, J.B.; Wiesenfeld, L. Possible observation of parity nonconservation by high-resolution NMR. *Europhys. Lett.* **1988**, *5*, 217–222.
22. Avetisov, V.A.; Goldanskii, V.I.; Kuz'min, V.V. Handedness, origin of life and evolution. *Phys. Today* **1991**, 33–41.
23. Latel, H. Parity Violation in Atomic Physics. In *Chirality - From Weak Bosons to the α -Helix*; Janoschek, R., Ed.; Springer: Berlin, Germany, 1992; Chapter 1, pp. 1–17.
24. Gardner, M. *The new ambidextrous universe - Symmetry and asymmetry from mirror reflections to superstrings*, 3rd ed.; Freeman: New York, NY, USA, 1990.
25. Bonner, W.A. Terrestrial and extraterrestrial sources of molecular homochirality. *Orig. Life Evol. Biosph.* **1991**, *21*, 407–420.
26. Salam, A. The role of chirality in the origin of life. *J. Mol. Evol.* **1991**, *33*, 105–113.
27. Orgel, L. Molecular replication. *Nature* **1992**, *358*, 203–209.
28. Kikuchi, O.; Kiyonaga, H. Parity-violating energy shift of helical *n*-alkane. *J. Mol. Struct.* **1994**, *312*, 271–274.
29. Bada, J.L. Origins of homochirality. *Nature* **1995**, *374*, 594–595.
30. Cline, D.B. *Physical Origin of Homochirality in Life*, AIP Conference Proceedings 379; AIP Press: Woodbury, NY, USA, 1996.
31. Avalos, M.; Babiano, R.; Cintas, P.; Jiménez, J.; Palacios, J.; Barron, L.D. Absolute asymmetric synthesis under physical fields: Facts and fictions. *Chem. Rev.* **1998**, *98*, 2845–2874.
32. Bailey, J.; Chrysostomou, A.; Hough, J.H.; Gledhill, T.M.; McCall, A.; Clark, S.; Ménard, F.; Tamura, M. Circular polarization in star-formation regions: Implications for biomolecular homochirality. *Science* **1998**, *281*, 672–674.
33. Pályi, G.; Zucchi, C.; Caglioti, L. *Advances in Biochemistry*; Elsevier: Amsterdam, The Netherlands, 1999.
34. Szabó-Nagy, A.; Keszthelyi, L. Demonstration of the parity-violating energy difference between enantiomers. *Proc. Natl. Acad. Sci. USA* **1999**, *96*, 4252–4255.
35. Feringa, B.L.; van Delden, R.A. Absolute asymmetric synthesis: the origin, control, and amplification of chirality. *Angew. Chem. Int. Ed.* **1999**, *38*, 3418–3438.
36. Avalos, M.; Babiano, R.; Cintas, P.; Jiménez, J.; Palacios, J. From parity to chirality: Chemical implications revisited. *Tetrahedron Assym.* **2000**, *11*, 2991–2404.
37. MacDermott, A.J. The ascent of parity-violation: Exochirality in the solar system and beyond. *Enantiomer* **2000**, *5*, 153–168.

38. Avalos, M.; Babiano, R.; Cintas, P.; Jiménez, J.L.; Palacios, J.C. Chiral autocatalysis: Where stereochemistry meets the origin of life. *Chem. Commun.* **2000**, 887–892.
39. Frank, P.; Bonner, W.A.; Zare, R. On One Hand But Not the Other: The Challenge of the Origin and Survival of Homochirality in Prebiotic Chemistry. In *Chemistry for the 21st Century*; Keinan, E., Schechter, E., Eds.; Wiley-VCH: Weinheim, German, 2001; Chapter 11, pp. 175–208.
40. Lough, L.W.; Wainer, I.W. *Chirality in Natural and Applied Science*; Blackwell: Oxford, UK, 2002.
41. Quack, M. How important is parity violation for molecular and biomolecular chirality? *Angew. Chem. Int. Ed.* **2002**, *41*, 4618–4630.
42. Shinitzky, M.; Nudelman, F.; Barda, Y.; Haimovitz, R.; Chen, E.; Deamer, D.W. Unexpected differences between D- and L-tyrosine lead to chiral enhancement in racemic mixtures. *Orig. Life Evol. Biosph.* **2002**, *32*, 285–297.
43. Crassous, J.; Chardonnet, C.; Saue, T.; Schwerdtfeger, P. Recent experimental and theoretical developments towards the observation of parity violation (PV) effects in molecules by spectroscopy. *Org. Biomol. Chem.* **2005**, *3*, 2218–2224.
44. Wagnière, G.H. *On Chirality and the Universal Asymmetry—Reflections in Image and Mirror Image*; Wiley-VCH: Weinheim, German, 2007.
45. Soai, K.; Kawasaki, T. Asymmetric autocatalysis with amplification of chirality. *Top. Curr. Chem.* **2008**, *284*, 1–33.
46. Guijarro, A.; Yus, M. *The Origin of Chirality in The Molecules of Life*; RSC: London, UK, 2009.
47. Fujiki, M. Mirror symmetry breaking of silicon polymers—From weak bosons to artificial helix. *Chem. Rec.* **2009**, *9*, 271–298.
48. Sozzi, M.S. *Discrete symmetries and CP violation: From experiment to theory*; Oxford University Press: Oxford, UK, 2008.
49. Wigner, E. Einige folgerungen aus der schroedingerschen theorie fur die termstrukturen. *Z. Phys.* **1927**, *43*, 624–652.
50. Wigner, E.P. *Symmetries and Reflections: Scientific Essays*; MIT Press: Cambridge, MA, USA, 1970.
51. Wigner, E.P. Violations of symmetry in physics. *Sci. Am.* **1965**, *213*, 28–36.
52. Adair, R.K. A flaw in a universal mirror. *Sci. Am.* **1988**, *258*, 30–36.
53. Wu, C.S.; Ambler, E.; Hayward, R.W.; Hoppes, D.D.; Hudson, R.P. Experimental test of parity conservation in beta decay. *Phys. Rev.* **1957**, *105*, 1413–1415.
54. Lee, T.D.; Yang, C.N. Question of parity conservation in weak interactions. *Phys. Rev.* **1956**, *105*, 254–258.
55. Nambu, Y.; Jona-Lasinio, G. Dynamical model of elementary particles based on an analogy with superconductivity. I. *Phys. Rev.* **1961**, *122*, 345–358.
56. Nambu, Y.; Jona-Lasinio, G. Dynamical model of elementary particles based on an analogy with superconductivity. II. *Phys. Rev.* **1961**, *124*, 246–254.
57. Weinberg, S. Conceptual foundations of the unified theory of weak and electromagnetic interactions. *Rev. Mod. Phys.* **1980**, *52*, 515–523.
58. Salam, A. Gauge unification of fundamental forces. *Rev. Mod. Phys.* **1980**, *52*, 525–538.
59. Glashow, S.L. Towards a unified theory: Threads in a tapestry. *Rev. Mod. Phys.* **1980**, *52*, 539–543.

60. Rubbia, C. Experimental observation of the intermediate vector bosons W^+ , W^- , and Z^0 . *Rev. Mod. Phys.* **1985**, *57*, 699–722.
61. Bouchiat, M.A.; Pottier, L. Optical experiments and weak interactions. *Science* **1986**, *234*, 1203–1210.
62. Frois, B.; Bouchiat, M.A. *Parity violation in atoms and polarized electron scattering*; World Scientific: London, UK, 1999.
63. Wang, W.; Yi, F.; Ni, Y.; Zhao, Z.; Jin, X.; Tang, Y. Parity violation of electroweak force in phase transitions of single crystals of D- and L-alanine and valine. *J Biol. Phys.* **2000**, *26*, 51–65.
64. Sullivan, R.; Pyda, M.; Pak, J.; Wunderlich, B.; Thompson, J.R.; Pagni, R.; Pan, H.; Barnes, C.; Schwerdtfeger, P.; Compton, R. Search for electroweak interactions in amino acid crystals. II. The Salam hypothesis. *J. Phys. Chem. A* **2003**, *107*, 6674–6680.
65. Wilson, C.C.; Myles, D.; Ghosh, M.; Johnson, L.N.; Wang, W. Neutron diffraction investigations of L- and D-alanine at different temperatures: The search for structural evidence for parity violation. *New J. Chem.* **2005**, *29*, 1318–1322.
66. Figgen, D.; Koers, A.; Schwerdtfeger, P. NWHClI: A small and compact chiral molecule with large parity-violation effects in the vibrational spectrum. *Angew. Chem. Int. Ed.* **2010**, *49*, 2941–2943.
67. Scolnik, Y.; Portnaya, I.; Cogan, U.; Tal, S.; Haimovitz, R.; Fridkin, M.; Elitzur, A.C.; Deamer, D. W.; Shinitzky, M. Subtle differences in structural transitions between poly-L- and poly-D-amino acids of equal length in water. *Phys. Chem. Chem. Phys.* **2006**, *8*, 333–339.
68. Lahav, M.; Weissbuch, I.; Shavit, E.; Reiner, C.; Nicholson, G.J.; Schurig, V. Parity violating energetic difference and enantiomorphous crystals-caveats; Reinvestigation of tyrosine crystallization. *Orig. Life Evol. Biosph.* **2006**, *36*, 151–170.
69. Figgen, D.; Schwerdtfeger, P. Structures, inversion barriers, and parity violation effects in chiral SeOXY molecules (X,Y=H, F, Cl, Br, or I). *J. Chem. Phys.* **2009**, *130*, 054306.
70. Kodona, E.K.; Alexopoulos, C.; Panou-Pomonis, E.; Pomonis, P.J. Chirality and helix stability of polyglutamic acid enantiomers. *J. Colloid Interf. Sci.*, **2008**, *319*, 71–80.
71. Fujiki, M.; Koe, J.R.; Terao, K.; Sato, T.; Teramoto, A.; Watanabe, J. Optically active polysilanes. Ten years of progress and new polymer twist for nanoscience and nanotechnology. *Polym. J.* **2003**, *35*, 297–344.
72. Fujiki, M. Switching handedness in optically active polysilanes. *J. Organomet. Chem.* **2003**, *685*, 15–34.
73. Fujiki M. Experimental tests of parity violation at helical polysilylene level. *Macromol. Rapid Commun.* **2001**, *22*, 669–674.
74. Dekkers, H.P.J.M. Circularly Polarized Luminescence: A probe for Chirality in the Excited State: In *Circular Dichroism: Principles and Applications*, 2nd ed.; Berova, N., Nakanishi, K., Woody, R.W., Eds.; Wiley-VCH: New York, NY, USA, 2000; Chapter 7.
75. Sato, T.; Terao, K.; Teramoto, A.; Fujiki, M. Molecular properties of helical polysilylenes in solution. *Polymer* **2003**, *44*, 5477–5495.
76. Laubender, G.; Berger, R. Ab initio calculation of parity-violating chemical shifts in NMR spectra of chiral molecules. *ChemPhysChem* **2003**, *4*, 395–399.

77. Weijo, V.; Manninen, P.; Vaara, J. Perturbational calculations of parity-violating effects in nuclear-magnetic-resonance parameters. *J. Chem. Phys.* **2005**, *123*, 054501.
78. Frisch, M.J.; Trucks, G.W.; Schlegel, H.B.; Scuseria, G.E.; Robb, M.A.; Cheeseman, J.R.; Montgomery, J.A., Jr.; Vreven, T.; Kudin, K.N.; Burant, J.C.; Millam, J.M.; Iyengar, S.S.; Tomasi, J.; Barone, V.; Mennucci, B.; Cossi, M.; Scalmani, G.; Rega, N.; Petersson, G.A.; Nakatsuji, H.; Hada, M.; Ehara, M.; Toyota, K.; Fukuda, R.; Hasegawa, J.; Ishida, M.; Nakajima, T.; Honda, Y.; Kitao, O.; Nakai, H.; Klene, M.; Li, X.; Knox, J.E.; Hratchian, H.P.; Cross, J.B.; Bakken, V.; Adamo, C.; Jaramillo, J.; Gomperts, R.; Stratmann, R.E.; Yazyev, O.; Austin, A.J.; Cammi, R.; Pomelli, C.; Ochterski, J.W.; Ayala, P.Y.; Morokuma, K.; Voth, G.A.; Salvador, P.; Dannenberg, J.J.; Zakrzewski, V.G.; Dapprich, S.; Daniels, A.D.; Strain, M.C.; Farkas, O.; Malick, D.K.; Rabuck, A.D.; Raghavachari, K.; Foresman, J.B.; Ortiz, J.V.; Cui, Q.; Baboul, A.G.; Clifford, S.; Cioslowski, J.; Stefanov, B.B.; Liu, G.; Liashenko, A.; Piskorz, P.; Komaromi, I.; Martin, R.L.; Fox, D.J.; Keith, T.; Al-Laham, M.A.; Peng, C.Y.; Nanayakkara, A.; Challacombe, M.; Gill, P.M.W.; Johnson, B.; Chen, W.; Wong, M.W.; Gonzalez, C.; Pople, J.A. *Gaussian 03, revision E.01*; Gaussian, Inc.: Wallingford, CT, USA, 2004.
79. Kamide, K.; Kataoka, A. Theoretical relationships between parameters in the Kuhn-Mark-Houwink-Sakurada equation. *Macromol. Chem. Phys.* **2003**, *128*, 217–228.
80. Carter, A.B.; Sanda, A.I. *CP* violation in *B*-meson decays. *Phys. Rev. D* **1981**, *23*, 1567–1579.
81. Aubert, B.; Boutigny, D.; Gaillard, J.M.; Hicheur, A.; Karyotakis, Y.; Lees, J.P.; Robbe, P.; Tisserand, V.; Palano, A.; Chen, G.P.; Chen, J.C.; Qi, N.D.; Rong, G.; *et al.* Observation of *CP* violation in the *B*⁰ meson system. *Phys. Rev. Lett.* **2001**, *87*, 091801.
82. Abe, K.; Abe, R.; Adachi, I.; Aihara, H.; Akatsu, M.; Alimonti, G.; Asai, K.; Asai, M.; Asano, Y.; Aso, T.; Aulchenko, V.; *et al.* Observation of large *CP* violation in the neutral *B* meson system. *Phys. Rev. Lett.* **2001**, *87*, 091802.

7. Appendix

Figure A1. UV and CD spectra in isoctane of (a) **3S** ($M_w = 232,000$, $M_n = 78,900$) at -86 °C and $+55$ °C, (b) **3R** ($M_w = 156,000$, $M_n = 76,800$) at -91 °C and $+55$ °C, (c) **4S** ($M_w = 14,500$, $M_n = 11,300$) at -61 °C and $+55$ °C, (d) **4R** ($M_w = 19,000$, $M_n = 15,200$) at -61 °C and $+55$ °C, (e) **5S** ($M_w = 42,300$, $M_n = 23,500$) at -82 °C and $+80$ °C, (f) **5R** ($M_w = 36,900$, $M_n = 19,000$) at -81 °C and $+15$ °C, (g) **6S** ($M_w = 108,000$, $M_n = 37,300$) at -5 °C and $+80$ °C, and (h) **6R** ($M_w = 80,900$, $M_n = 34,600$) at -5 °C and $+80$ °C.

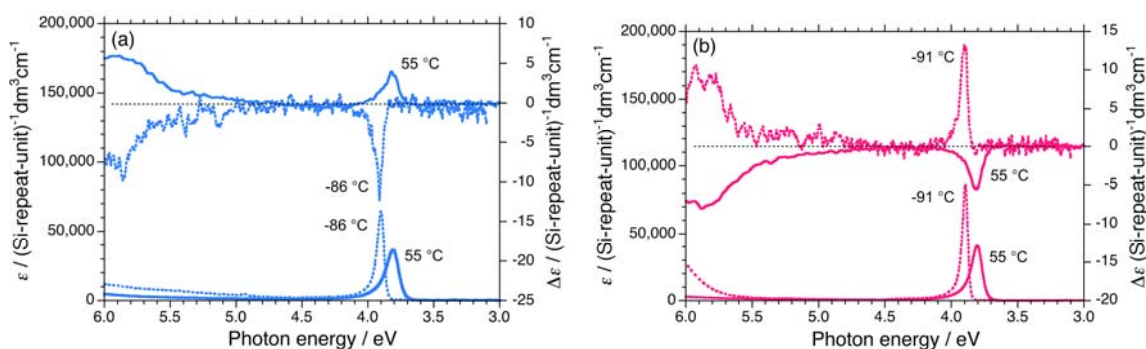


Figure A1. Cont.

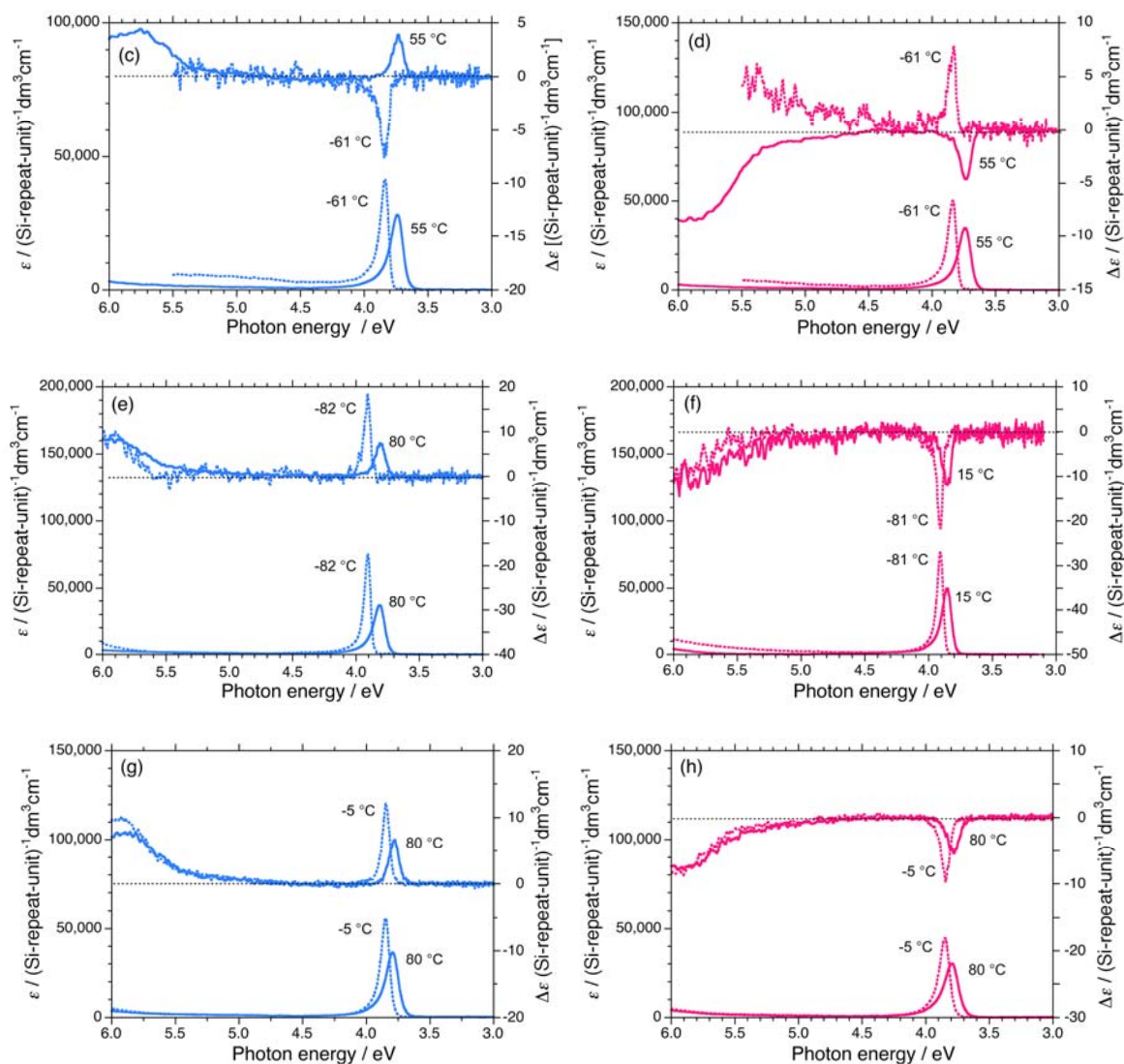
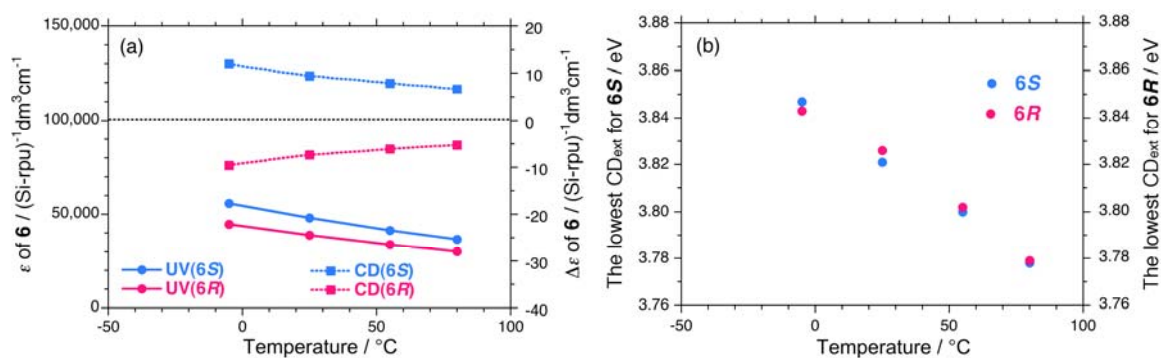


Figure A2. (a) Absorptivity (ϵ) and CD signal ($\Delta\epsilon$), and (b) apparent CD extrema near 3.9 eV of **6S** ($M_w = 108,000$, $M_n = 37,300$) and **6R** ($M_w = 80,900$, $M_n = 34,600$) in isoctane as a function of temperature.



Scheme A1. Synthetic scheme of **1S** and **1R**. For **2S/2R**, **3S/3R**, **4S/4R**, and **5S/5R**, the corresponding organotrichlorosilane (Shin-Etsu) was used. For synthesis of **6S/6R**, *n*-dodecyltrichlorosilane (Shin-Etsu), (*S*)-2-methylchloride (TCI), and (*R*)-2-methylchloride (synthesized by Chemical Soft, Kyoto, Japan) were used as starting materials.

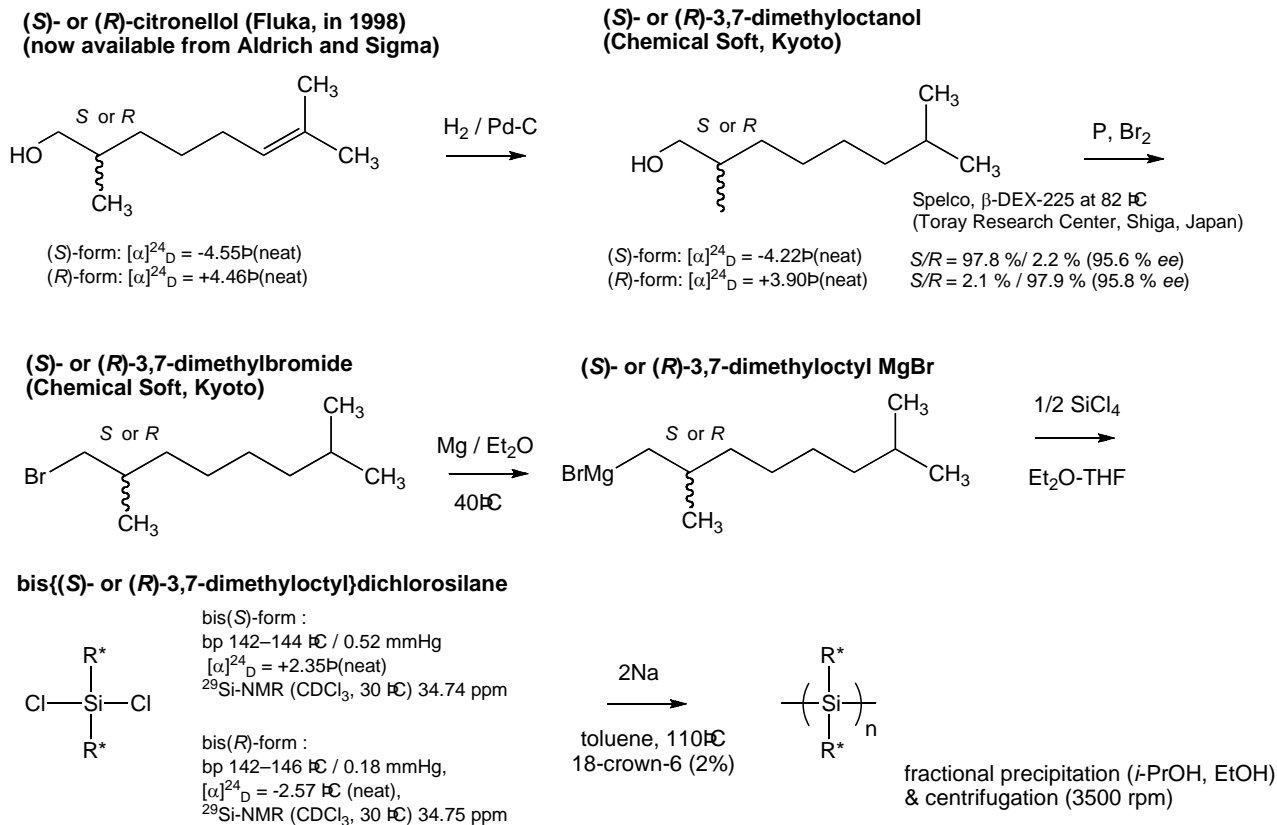


Figure A3. Gas chromatography (GC) charts of (*S*)-(-)-3,7-dimethyloctanol and (*R*)-(+)-3,7-dimethyloctanol. Measurement and analysis were carried out at TRC (Shiga, Japan) by the chiral GC method (Supelco, β-DEX-225, 30 m x 0.25 mm ID, column oven 82 °C, He carrier with 1.2 mL/min).

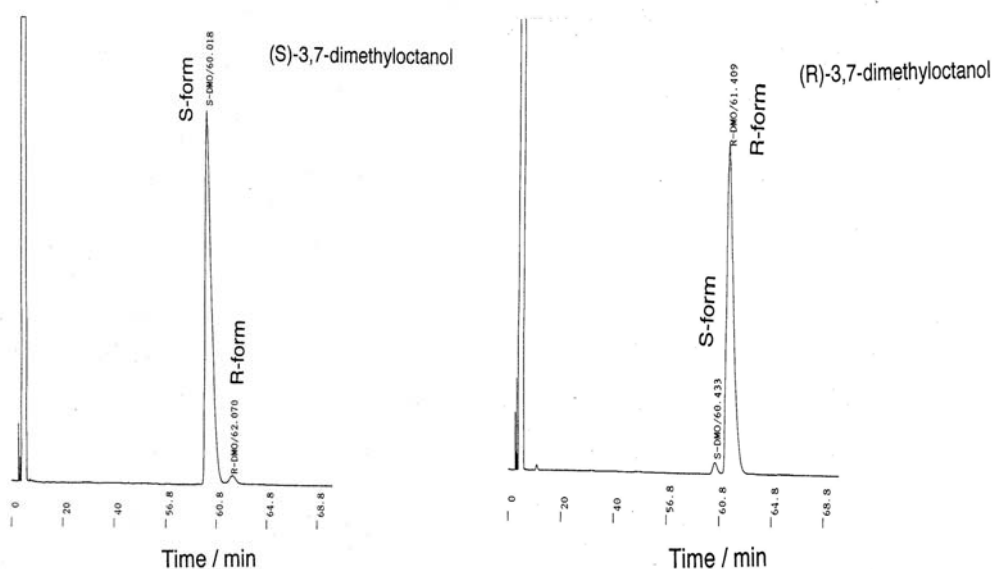
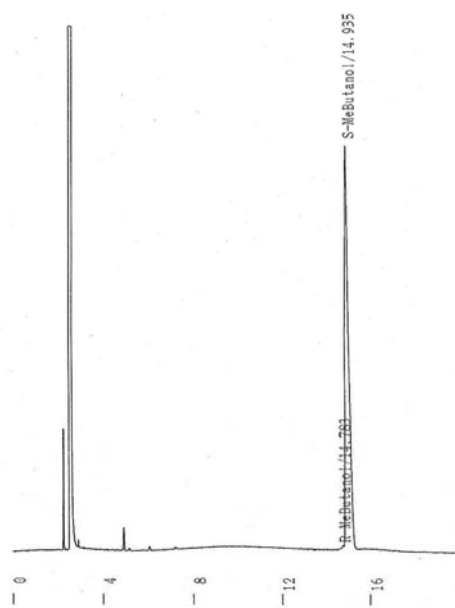


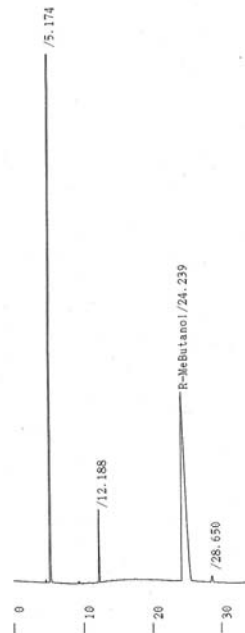
Figure A4. GC charts of (*S*)-(+)-2-methylbutanol and (*R*)-(+)-2-methylbutanol. Measurement and analysis were done by TRC with the chiral GC method (Supelco, β -DEX-325, 30 m x 0.25 mm ID, column oven 55 °C, He carrier with 1.2 mL/min).



** 定量的計算結果 **

CH	PKNO	TIME	AREA	HEIGHT	MK	IDNO	CONC	NAME	
1	2	14.783	72	5	1	1	0.2448	R-MeButanol	
3	3	14.935	8944	765	2	2	99.7552	S-MeButanol	
TOTAL							8986	770	100

図4 TCI (*S*)-2-methyl-1-butanolのガスクロマトグラム
(カラム: β -DEX325、カラム温度: 55°C)



** 定量的計算結果 **

CH	PKNO	TIME	AREA	HEIGHT	MK	IDNO	CONC	NAME	
1	1	5.174	295699	76828	1	1	100	R-MeButanol	
4	4	12.188	1793	218	1	1	100	R-MeButanol	
5	5	24.239	2718	25	1	1	100	R-MeButanol	
6	6	28.650	339	25	1	1	100	R-MeButanol	
TOTAL							325298	77850	100

図2 Chemical Soft (*R*)-2-methyl-1-butanol + (*R*)-2-methylbutylchlorideのガスクロマトグラム
(カラム: β -DEX325、カラム温度: 55°C)

© 2010 by the authors; licensee MDPI, Basel, Switzerland. This article is an Open Access article distributed under the terms and conditions of the Creative Commons Attribution license (<http://creativecommons.org/licenses/by/3.0/>).